Binocular luster elicited by isoluminant chromatic stimuli relies on mechanisms similar to those in the achromatic case

Gunnar Wendt Universität Kiel, Kiel, Germany

Franz Faul Universität Kiel, Kiel, Germany

The phenomenon of binocular luster can be evoked by simple dichoptic center-surround stimuli showing a luminance contrast difference between the eyes. Previous findings support the idea that this phenomenon is mediated by a low-level conflict mechanism that integrates the monocular signals from different types of contrast detector cells. Also, isoluminant stimuli with different chromatic contrasts between eyes can trigger sensations of luster. Here, we investigate whether the lustrous impression in such purely chromatic stimuli depends on interocular contrast differences and in particular on interocular contrast polarity pairings in a similar way as in the achromatic case. In our experiments, we measured the magnitude of the lustrous response using a series of isoluminant dichoptic center-ring-surround stimuli with varying ring width whose chromatic properties were varied along the red–green and blue–yellow cardinal directions. The trends in the data were very similar to those of our former study with achromatic stimuli, indicating similar mechanisms in both cases. The empirical luster data could also be predicted fairly well by a chromatic version of our interocular conflict model (with overall R^2 values between 0.577 and 0.639), for which two different receptive field models were used, simulating the behavior of color-sensitive double-opponent cells in V1.

Introduction

Binocular luster is a visual phenomenon that can be produced with simple dichoptic stimuli. Typically, center-surround stimuli are used in which the center patches differ in luminance between eyes, and the luminance of the surround is identical in both monocular half-images. The center area in the cyclopean view can then assume a peculiar appearance that is often described as lustrous, glassy, or even self-luminous (Wendt & Faul, 2020; Wendt & Faul, 2022b). The strength of the impression depends on the sign of the contrast between center and surround: Center-surround stimuli showing the same contrast polarity in each eye—that is, when the two eyes are presented with different spatial increments (inc–inc stimulus pair in Figure 1) or different spatial decrements (Formankiewicz & Mollon, 2009; Sheedy & Stocker, 1984; Zhang, 2015)—elicit only weak lustrous impressions. The perceived luster is considerably stronger in stimuli with reversed contrast polarities—that is, when a spatial increment is dichoptically combined with a spatial decrement, as in the inc–dec stimulus pair in Figure 1 (e.g., Anstis, 2000; Georgeson, Wallis, Meese, & Baker, 2016; Hetley & Stine, 2019; Venkataramanan, Gawde, Hathibelagal, & Bharadwaj, 2021; Wendt & Faul, 2019; Wendt & Faul, 2022a; Wolfe & Franzel, 1988).

As an explanation for this finding, Anstis (2000) suggested that binocular luster is mainly the result of a neural conflict that is caused by the inability of the visual system to binocularly combine monocular signals produced by two different kinds of retinal ganglion cells (see also Georgeson et al., 2016). These cell types, whose receptive field has a circular-symmetric antagonistic center-surround structure, are referred to as ON- or OFF-center cells. The central area of the ON-center cell is excitatory and its surround inhibitory, which makes it sensitive to incremental luminance patterns in the retina, whereas the OFF-center cell, in which this spatial relation is reversed, is responsive to decremental luminance patterns (Schiller, 1992; Wienbar & Schwarz, 2018). Inc–dec stimuli would trigger these two different types of ganglion cells at corresponding retinal locations (Figure 1, top row).

According to Anstis (2000), the visual system is unable to integrate these two monocular signals at a binocular level, and they therefore remain in a state of competition, causing the phenomenon of luster (similar conflict ideas have already been proposed by Brewster, 1861, and Sachsenweger, 1960; see also Mausfeld, Wendt, & Golz, 2014; Wendt & Faul, 2022b). Alternatively, there may be binocular cells in the early visual system that specifically respond

Citation: Wendt, G., & Faul, F. (2024). Binocular luster elicited by isoluminant chromatic stimuli relies on mechanisms similar to those in the achromatic case. *Journal of Vision*, *24*(3):7, 1–26, https://doi.org/10.1167/jov.24.3.7.

https://doi.org/10.1167/jov.24.3.7 Received December 12, 2023; published March 27, 2024 ISSN 1534-7362

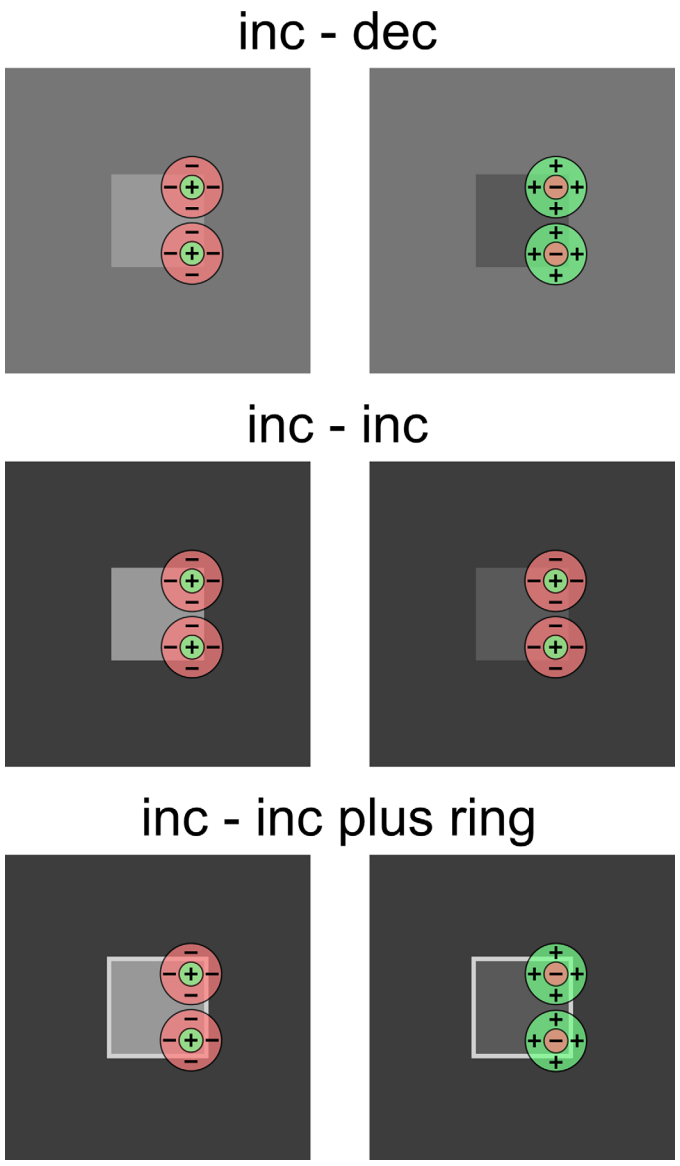

Figure 1. In the top row, an inc–dec stimulus pair is shown that produces strong sensations of luster in the center patch area of the fused percept. According to Anstis (2000), this is due to the fact that different types of retinal ganglion cells with antagonistic center-surround receptive fields (ON- and OFF-center cells) are stimulated at corresponding locations whose signals cannot be combined at a binocular level. Inc–inc stimuli (middle row) exclusively trigger ON-center cells at corresponding retinal positions. The lustrous impression elicited by such stimuli is much weaker. However, when the center patches of the inc–inc stimuli are enclosed by a thin light ring (bottom row), the magnitude of the lustrous response is considerably increased—possibly due to the fact that the ring and surround luminances are spatially integrated by the surround area of the receptive fields of the ganglion cells such that, at some locations within the target area, luster-enhancing ON–OFF pairings are produced between eyes.

to interocular conflicts, particularly to between-eye luminance patterns with reversed contrast polarities (Kingdom, Read, Hibbard, & May, 2022); we discuss this idea in more detail in the General Discussion section. Support for this idea has been provided by, for example, Kingdom, Jennings, and Georgeson (2018), who showed that the mechanism underlying the phenomenon of binocular luster is adaptable. Generally, there is a growing body of evidence showing that such conflict-sensitive neurons, whose purpose is to detect interocular discrepancies, also play a role in other binocular phenomena such as stereopsis (Goncalves & Welchman, 2017; Read & Cumming, 2007) and binocular rivalry (Katyal, Engel, He, & He, 2016; Katyal, Vergeer, He, He, & Engel, 2018; Said & Heeger, 2013), which is assumed to be closely related to binocular luster (Wendt & Faul, 2022b).

In recent studies, we provided some support for the conflict approach (Wendt & Faul, 2020; Wendt & Faul, 2022a). For example, in some of our psychophysical experiments we measured the strength of perceived luster using a series of dichoptic center-ring-surround stimuli. Four different combinations of ring-surround luminances were used, which were chosen such that the center patch luminances were characterized by different interocular contrast polarity combinations (Figure 2, top row). In addition, the width of the ring was systematically varied. When the empirical luster judgments were plotted as a function of ring width, characteristic curves resulted for the four different ring-surround luminance conditions (Figure 2, bottom row).

In particular, we found that the addition of a thin ring adjacent to the center patch leads to a strong increase in perceived luster when the two center patches are (a) both incremental (or both decremental) to the surround luminance and at the same time (b) both decremental (or incremental) to the ring luminance (see the two consistent conditions in Figure 2). Our interpretation of the luster-enhancing effect of the thin ring is as follows: Although, at the stimulus level, the two center patches have consistent contrast polarities to both the surround and ring element, this stimulus configuration partially stimulates ON- and OFF-center cells at corresponding retinal locations, because their receptive fields spatially integrate the ring and surround luminances (see also the bottom stimulus pair in Figure 1). However, larger rings eventually exceed the range of the receptive fields of these cells and then take on the role of the surround, resulting in simple inc–inc or dec–dec stimulus configurations that trigger much weaker lustrous sensations.

In fact, our empirical data could be well predicted by a simple interocular conflict model based on the between-eye interaction of the signals of the ON- and OFF-center cells (with a proportion of explained

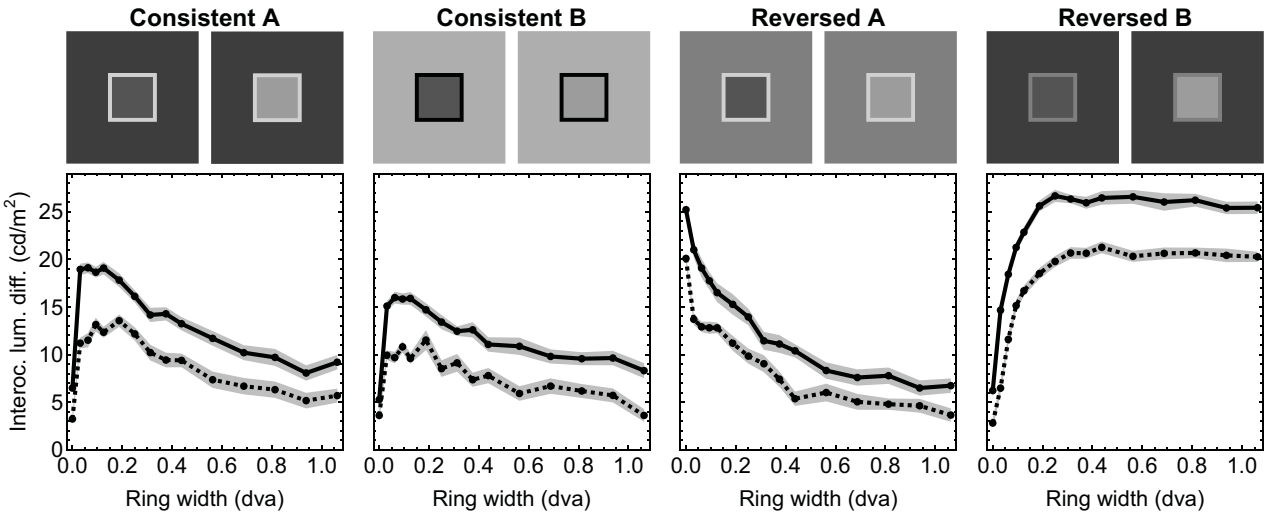

Figure 2. Results of one of our previous experiments in which the strength of perceived luster was measured using achromatic stimuli (Experiment 1 in Wendt & Faul, 2022a). We used four different combinations for the ring and the surround luminance that produced different interocular contrast polarity combinations with regard to the two center patch luminances (top row). In each of these four contrast conditions, the width of the ring was varied, and two different dichoptic luminance differences for the center patches were used. The bottom row shows the results of the matching experiment averaged across all subjects. The luster settings are plotted as a function of ring width. The data for the center patches with a higher dichoptic luminance difference are shown as solid curves, those for the lower dichoptic difference as dotted curves. Transparent areas represent 1 *SEM* in both directions.

variance of more than 80%). These results are consistent with the idea that the between-eye interaction of specific kinds of contrast or edge detector cells, such as the retinal ganglion cells, plays a crucial role in the generation of a lustrous response. To account for weaker lustrous impressions elicited by stimuli with consistent contrast polarities between eyes, the latest incarnation of our model not only is based on interocular ON–OFF pairings but also includes ON–ON and OFF–OFF pairings (Wendt & Faul, 2022a). However, the contribution of these two consistent contrast signal combinations to the overall conflict measure is much weaker compared with the ON–OFF signal pairings.

Binocular luster in chromatic stimuli

From the very beginning of the investigation of the phenomenon of binocular luster, it was found that a lustrous impression, albeit considerably weaker, can also be produced with color stimuli in which all stimulus elements are isoluminant (e.g., Dove, 1851; Jennings & Kingdom, 2016; Jung, Moon, Park, & Song, 2013; Kiesow, 1920; Malkoc & Kingdom, 2012; von Helmholtz, 1867; Wendt & Faul, 2019; Wundt, 1862; Yoonessi & Kingdom, 2009). This raises a number of questions that we will deal with in this study: (1) Do the lustrous sensations produced with pure chromatic stimuli depend on interocular contrast polarity combinations in a similar way as in the achromatic case? (2) Is it possible to predict the magnitude of the lustrous response in the chromatic case with a modified version of our interocular conflict model? (3) Are there any indications of what color-sensitive neural mechanisms are involved in the generation of a lustrous impression with chromatic stimuli?

General methods

In order to address the above questions, we first conducted two psychophysical experiments, following the same approach as in our former study (Wendt & Faul, 2022a). That is, we measured the magnitude of the lustrous sensation elicited by a family of isoluminant dichoptic center-ring-surround stimuli, which varied in their chromatic properties and the width of the ring. Note that, in the present study, we conducted chromatic versions of only two of the four experiments of our previous study. As the lustrous effect with chromatic stimuli is expected to be weaker than with achromatic stimuli (Jung et al., 2013; Wendt & Faul, 2019; Wendt & Faul, 2022b), we decided to use only chromatic variants of those experiments of the original study that showed a comparatively high variability in the magnitude of the lustrous responses across the different stimulus conditions.

Subjects

Six subjects (three female and three male) participated in Experiment 1, five of them also in Experiment 2. One of the participants was an author of this study (GW). All subjects had normal or corrected-to-normal visual acuity and normal color vision, as tested by means of the Ishihara (1967) plates. Prior to the experiments, the subjects gave written consent and were informed about their rights, tasks, and potential risks of their participation in this study.

Apparatus

The stimuli were presented on a 24-inch CG243W monitor (EIZO, Ishikawa, Japan) with a resolution of 1920 × 1200 pixels. We applied a standard procedure to calibrate the monitor (Brainard, 1989) using a JETI specbos 1211 spectroradiometer (JETI Technische Instrumente GmbH, Jena, Germany). In order to fuse the two half-images of the dichoptic stimuli, which were presented side-by-side on the screen, we used a mirror stereoscope (ScreenScope; Stereo Aids, Albany, WA, Australia). The stereoscope was mounted to the monitor and adjusted such that the viewing distance was 50 cm. In each trial during the experiment, the test stimulus was always displayed together with a comparison stimulus (either an anchor or a matching stimulus; see Procedure section). The two stimuli were arranged such that the test appeared in the top half of the monitor and the comparison at the bottom half, with a vertical center-to-center distance of 13.7 degrees of visual angle (dva).

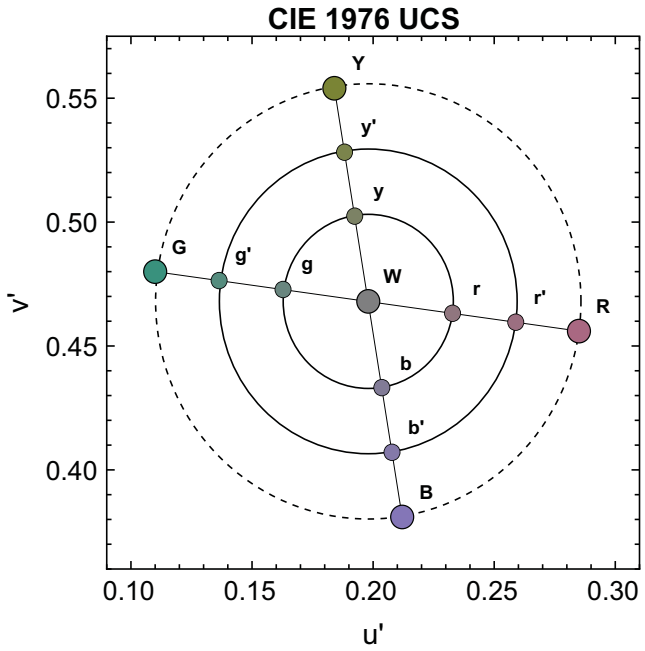

Figure 3. The chromaticity coordinates for the two color conditions in the CIE 1976 UCS diagram. The red–green color condition is defined by the line segment with the two endpoint colors R and G and the blue–yellow color condition by the line segment with the endpoints B and Y. All endpoint colors have the same distance to the central neutral point W. In our color scheme, the endpoint colors define a unit circle (dashed), which is used to determine the color positions of further colors, such as those of the center patch colors. In Experiment 1, we used two dichoptic pairs of colors for the center patches in each of the two color conditions. One of the center patch color pairs had a dichoptic color difference (DCD) of 0.4 relative units (r–g and b–y; that is, the distance from the central white point W was 0.4 relative to their corresponding endpoints); the other had a DCD of 0.7 (r'–g' and b'–y').

Stimuli

As our aim was to test whether the lustrous responses in pure chromatic stimuli are affected similarly by interocular (cone) contrast polarity combinations and by interocular luminance polarity combinations (Wendt & Faul, 2020; Wendt & Faul, 2022a), we used isoluminant dichoptic center-ring-surround configurations as test stimuli, where all stimulus elements had a luminance of 25 cd/m^2. The square center patches had a constant side length of 2.0 dva (equivalent to 64 pixels for our viewing conditions), whereas the rings, which were also square shaped and adjacent to the center patch, had variable widths. These center-ring combinations were embedded in a large surround that fully occupied the respective upper or lower half of the monitor screen.

We tested two color conditions that correspond to the cardinal axes in color space (which are parallel to the *r* and *b* axes of the MacLeod-Boynton chromaticity diagram) (MacLeod & Boynton, 1979). Each of the two color conditions was defined by a line segment in the CIE 1976 u′,v′ uniform chromaticity scale (UCS) chromaticity diagram, determined by two endpoint colors, all having the same distance to the central white point (W; see Figure 3) which represents D65 (u′,v′,L = 0.198, 0.468, 25). The distances to the neutral point were chosen such that the endpoints were close to the gamut of the monitor used in the experiments. In one condition, which we refer to as the red–green (RG) condition, the line segment was defined by the endpoints R (u′,v′,L = 0.285, 0.456, 25) and G (u′,v′,L = 0.110, 0.480, 25). The other color condition, blue–yellow (BY), was determined by endpoints B (u′,v′,L = 0.212, 0.381, 25) and Y (u′,v′,L = 0.184, 0.554, 25). In one of our previous studies on binocular luster with color stimuli (Wendt & Faul, 2019), we showed that, by varying the

positions of the two center patch colors relative to the color position of the surround element along a line segment, the interocular combinations of cone contrast polarities in simple dichoptic center-surround stimuli could be systematically varied. For example, reversed contrast polarities between the two center patches could be produced when the surround color was located between the two center patch colors on the line segment. In the RG case, this would produce interocular inc–dec combinations regarding the L and M cone excitations and in the BY case regarding the S cone excitations. Stimuli with consistent cone contrast polarities between eyes (i.e., inc–inc or dec–dec combinations) could be produced with colors for the two center patches that are both located in the same direction relative to the color position of the surround element on the color line segment.

The endpoint colors R, G, B, and Y determine the unit circle in our color scheme (see Figure 3). For a more intuitive representation of colors used in the experiments, all colors are defined by their relative color distance to the neutral point in the direction of their corresponding endpoint.

Procedure

In order to measure the magnitude of the lustrous impression evoked by the target area of the test stimulus (which corresponds to the center patch area in the fused stimulus), we employed two different methods in each trial (Wendt & Faul, 2020; Wendt & Faul, 2022a). First, the test stimulus was presented together with an anchor stimulus, and the subject had to judge the perceived strength of the lustrous impression in the test stimulus on a rating scale using integer values between 0 (corresponding to a non-lustrous or matte appearance) and 5 (corresponding to a maximally lustrous appearance). The anchor stimulus was used to provide the subject with a matte reference, such that even subtle degrees of luster in the test stimulus could be easily detected. The ring and the surround colors of the anchor stimulus were identical to those of the test stimulus. In order to produce a matte appearance in the target area of the anchor stimulus, both center patches had the same color, which was D65, with a luminance that was slightly lower than what we used for the patches of the test (u',v',L = 0.198, 0.468, 22.5). This way, the center patch area of the anchor was still discernible from neighboring stimulus elements in cases where these elements were set to a neutral color. After the subject selected the rating value, which was displayed at the top of the test stimulus and which could be interactively changed using the up or down keys of the keyboard, he or she could end the rating task by pressing the space bar.

Generally, after a dark adaptation period of 1 second, the second task started where the same test stimulus as before was displayed (still in the upper half of the screen) together with a match stimulus. However, the matching task was only applied in cases where the test stimulus rating was greater than 0. Otherwise, the matching part was skipped (with the interocular luminance difference stored with a value of 0; see below), and the next trial began. The match stimulus was achromatic with a surround luminance of 10 cd/m^2 and a ring of constant width of 0.125 dva (equivalent to 4 pixels) with a luminance of 25 cd/m^2. The interocular luminance difference of its center patches could be interactively manipulated by the subject, using the left and right keys on the keyboard. This manipulation systematically alters the magnitude of the lustrous sensation, and the task of the subject was to find the setting that made the perceived strength of the lustrous impression in the match stimulus as similar as possible to the one in the test stimulus. The two center patch luminances C_l and C_r were calculated as follows:

$$C_{l,r} = 25 * \left(1 \pm \alpha^k\right) \text{ cd/m}^2,$$
$$\text{for } 0 <= \alpha <= 1 \text{ and } k = 1/0.77.$$

The subjects adjusted the value of α, and the exponent k was chosen to ensure an approximately linear relationship between α and the strength of perceived luster (Wendt & Faul, 2019). Using this match stimulus allows us to directly compare the luster settings between the two different color conditions of the present study. Moreover, because we already used the same match stimulus in our previous experiments (Wendt & Faul, 2022a) (Figure 2), it is possible to compare the present results with those of our former study, in which only achromatic stimuli were examined.

Prior to the start of Experiment 1, each subject was carefully instructed on the procedure and was presented with four example stimuli selected to present the full range of lustrous sensations. Because binocular luster is generally a rather unstable phenomenon for which the perceived strength tends to vary over time (cf. Qiu, Caldwell, You, & Mendola, 2020; Ruete, 1860; Sachsenweger, 1960; Wendt & Faul, 2022b), subjects were asked to base their judgment on the maximum perceived luster during the stimulus presentation (the duration of which was not time limited). It should be noted that this instability is especially pronounced for stimuli without a ring or with larger ring widths, whereas thin rings seem to have a stabilizing effect on the lustrous sensation (Wendt & Faul, 2020; Wendt & Faul, 2022b). As a means of restoring luster, subjects were asked not to fixate the stimuli for prolonged periods but to keep their eyes moving (Howard, 1995; Sachsenweger, 1960).

Experiment 1

The first experiment is the equivalent to Experiment 1 of our former study (Wendt & Faul, 2022a), in which we examined the effect of the ring width on perceived luster. A further question addressed in our previous study was how the lustrous impression depends on four different combinations of ring and surround luminances, which produced different combinations of interocular contrast polarity combinations with respect to the two center patch luminances (see Figure 2). A similar approach was employed in the present experiment: For each of the two color conditions RG and BY, we tested four different color combinations for the ring and the surround element, each based on the two endpoint colors of the respective color condition and the common white point (Figure 4): In condition 1, we used the first endpoint color (R or B) for the ring and the second endpoint color (G or Y) for the surround. In condition 2, we just swapped these color relations between ring and surround so that the second endpoint color (G or Y) was used for the ring and the first endpoint color (R or B) was used for the surround. In condition 3, we used the first endpoint color for the ring and the color of the neutral point (W) for the surround. Finally, in condition 4, the neutral point color (W) was used for the ring and the endpoint color 2 was used for the surround.

We tested two pairs of center patch colors with different dichoptic color differences (DCDs) in each of the two color conditions, RG and BY. For the lower DCD, the relative color distance was 0.4; for the higher DCD, it was 0.7 (denoted with lower case letters in Figure 3). In contrast conditions 1 and 2, these two center patch colors were, in terms of the respective cone excitations, either both incremental (or decremental) to the surround color and at the same time both decremental (or incremental) to the ring color. We therefore refer to these conditions as *Consistent A* and *Consistent B*, respectively (Figure 3). In the two remaining contrast conditions, the two center patches either had reversed contrast polarities with respect to the surround color (condition 3) or with respect to the ring color (condition 4). We refer to these conditions as *Reversed A* and *Reversed B*, respectively. The ring was tested with eight different widths: 0, 0.0625, 0.125, 0.25, 0.375, 0.5625, 0.8125, and 1.0625 dva (equivalent to 0, 2, 4, 8, 12, 18, 26, and 34 pixels, respectively).

Each of the 128 different condition combinations (2 color conditions × 4 contrast conditions × 2 center patch conditions × 8 ring widths) was tested eight times. The 1024 test stimuli were presented in random order. To account for possible effects of ocular dominance, the center patch colors of the left and right half-images were swapped in half of the trials of each condition combination.

Results

The results of Experiment 1 are shown in Figure 5. These results are based on averaged values of all subjects. In Appendix A, the results of the rating task (Figure A1) and the matching task (Figure A2) are shown for individual subjects. In each figure, the dependent variable is plotted as a function of ring width. The rows depict the results of different subjects, and the columns show the results in the four different contrast conditions (Consistent A and B; Reversed A and B). In each diagram, the two color conditions are indicated by different colors of the curves (red for the RG color condition and blue for the BY color condition). The two amounts of dichoptic color difference realized in the experiment are indicated by dashed lines (low DCD) and solid lines (high DCD). The mean rating and the matching values were highly correlated, with Pearson's correlation coefficients for the individual datasets ranging between 0.92 and 0.975 for color condition RG and between 0.917 and 0.979

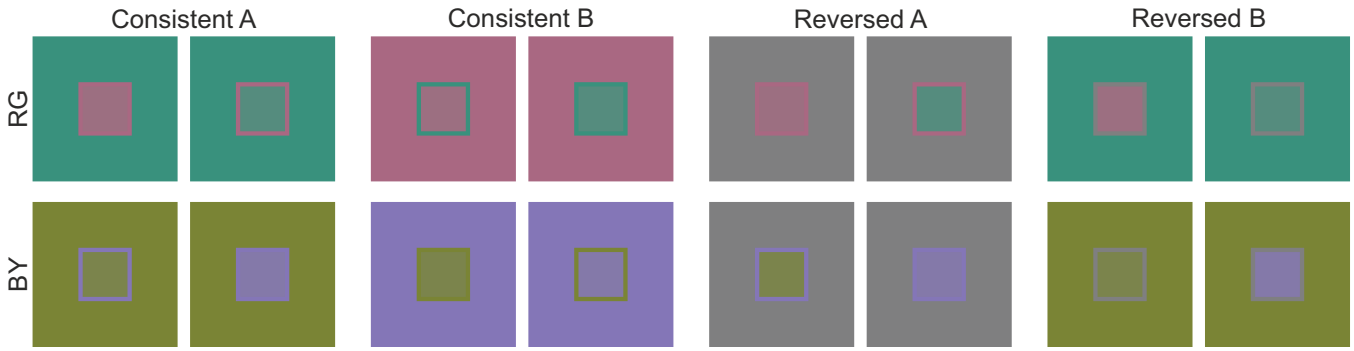

Figure 4. Stimulus conditions realized in Experiment 1. For each of the two color conditions RG and BY (rows), four different contrast conditions were used with different combinations for the ring and the surround chromaticities. As an additional factor, the width of the ring was systematically varied. See main text for further details.

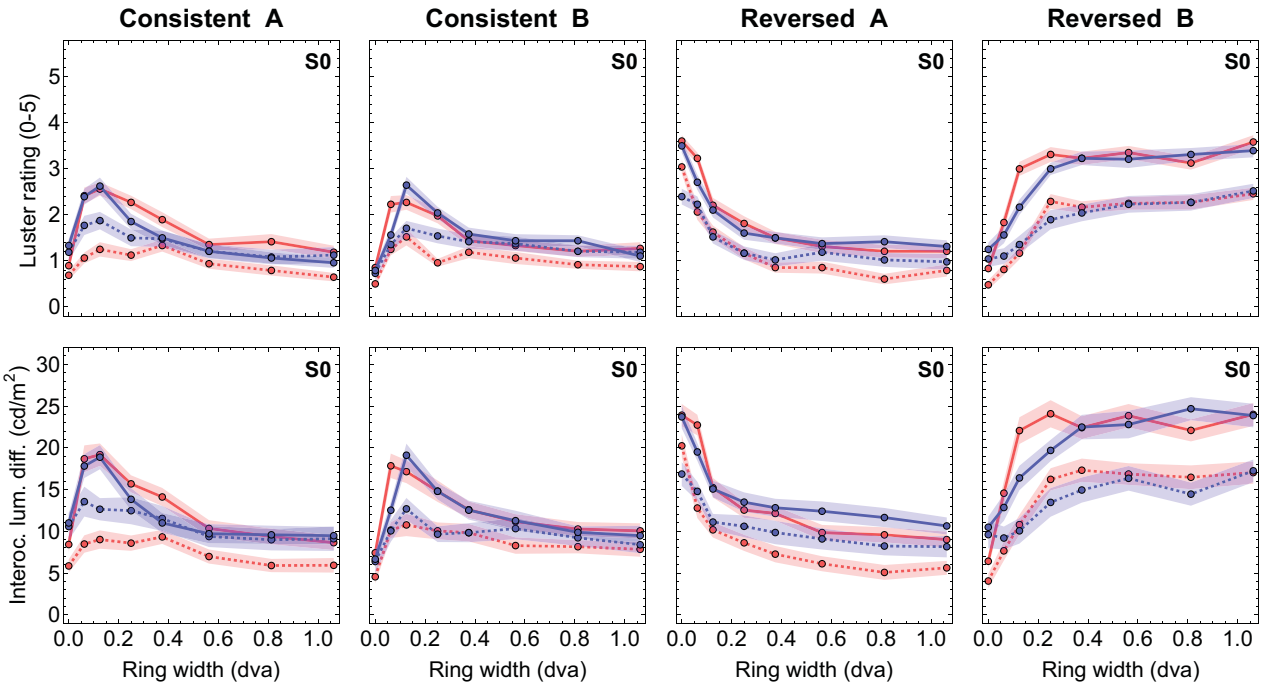

Figure 5. Results of the rating (top row) and the matching task (bottom) of Experiment 1 for the pooled data (S0). For each contrast condition (columns), the respective dependent variable is plotted as a function of ring width. Red curves show the results for the RG color condition, blue curves those for the BY color condition. Solid lines refer to the high DCD condition, dashed lines to the low DCD condition. Transparent areas represent 1 *SEM* in both directions.

for color condition BY. Averaged across all subjects, these correlation coefficients were $r = 0.959$ for the RG condition and $r = 0.968$ for the BY condition. It should be noted, though, that these strong correlations could also be partly due to the fact that the matching task immediately followed the rating task. This carries the risk that the subject does not base the matching (which is a comparatively difficult task) exclusively on the lustrous impression perceived in the test stimulus but also on the previously assigned rating value. It is therefore quite possible that the two procedures are not completely independent measurements of perceived luster.

Generally, the trends in both color conditions are similar to those found in our previous study with achromatic stimuli (see Figure 2). For example, in the two Consistent conditions, the peak of the lustrous response occurred at small ring widths, whereas the no-ring condition and larger ring widths led to markedly weaker lustrous sensations. The data obtained under the two Reversed conditions are also consistent with our previous results: In the Reversed A condition, the polarity of the contrast of the two center patch colors to the surround color was reversed and this produced strong sensations of luster when no ring was added. However, because both center patches had consistent contrast polarities with regard to the ring color, an increase in ring width led to a continuous decrease in perceived luster. These interocular contrast polarity relations are reversed in the Reversed B condition, resulting in the opposite effect—that is, a continuous increase in the magnitude of the lustrous response with increasing ring width (up to a certain limit at which the strength of perceived luster reaches a nearly constant level). Furthermore, as expected, luster ratings and luster settings were generally higher when the center patches had a higher dichoptic color difference (high DCD) than when this difference was lower (low DCD) (see Table 1).

Only subject S3 (Figures A1 and A2) showed a somewhat surprising pattern of results in this regard: For the BY color condition in particular, the stimuli from the low DCD condition were mostly judged to be more lustrous than those from the high DCD condition. Consequently, this subject also showed a significant interaction effect between the two factors color and DCD (Table 1). It should be noted that this subject also generally produced considerably higher standard deviations than the other subjects.

Interestingly, the present results contradict previous reports that perceived luster in pure chromatic stimuli is much weaker than for stimuli that show luminance differences between eyes (Jung et al., 2013; Pieper & Ludwig, 2001; Wendt & Faul, 2019; Wendt & Faul, 2022b)—this is true at least with regard to the averaged data. Such a direct comparison of the magnitude of

	Color condition			DCD			IA	Non-lustrous (%)			
Subject	RG	BY	*p*	Low DCD	High DCD	*p*	*p*	RG (Low DCD)	RG (High DCD)	BY (Low DCD)	BY (High DCD)
S1	7.44	9.35	<0.001	6.51	10.28	<0.001	0.191	34.77	11.72	16.02	3.90
S2	10.78	13.61	<0.001	9.84	14.55	<0.001	0.344	12.50	6.25	1.95	0.00
S3	13.00	25.66	<0.001	18.48	20.18	0.027	<0.001	44.92	33.98	1.56	3.90
S4	10.83	5.88	<0.001	4.51	12.20	<0.001	0.002	58.98	21.09	72.66	46.88
S5	12.56	6.76	<0.001	7.61	11.70	<0.001	0.120	1.17	0.78	39.45	12.89
S6	19.63	16.43	<0.001	15.91	20.15	<0.001	0.370	3.13	2.73	4.30	1.56
S0	**12.37**	**12.95**	**.017**	**10.45**	**14.85**	**<0.001**	**<0.001**	**25.91**	**12.76**	**22.66**	**11.52**

Table 1. The table shows, separately for the individual matching datasets (S1—S6) and for the pooled matching data (S0), parts of a four-way ANOVA with a focus on effects due to color differences. Therefore, only the results for the two factors of color condition (columns 2–4) and dichoptic color difference (DCD, columns 5–7), as well as the significance level of the interaction effect between them (IA, column 8), are presented. In the remaining columns 9 to 12, the proportions of the non-lustrous judgments are shown separately for the two color conditions and the two DCD levels, respectively.

the lustrous responses is possible because we used the same match stimulus in the present study as in our former study with achromatic stimuli. A comparison of Figures 2 and 5, which show the mean data of both studies, reveals that corresponding curves of the previous and the present study are very similar not only with respect to their general shape but also regarding the range of values. However, both aspects differ significantly between subjects and also between the two color conditions.

Our data reveal some interesting differences among subjects with regard to their sensitivity to the luster phenomenon in purely chromatic stimuli. Table 1 shows partial results of a four-way ANOVA (color condition × contrast condition × DCD × ring width) based on the matching data, separately for all individual datasets as well as for the data averaged across all subjects. In the table, only those effects related to the influence of the color condition and the DCD on the luster settings are shown. In addition, the proportions of stimuli that were perceived as non-lustrous are shown. If we consider these proportions, there are subjects (such as S2 and especially S6) who judged the vast majority of the stimuli (between 90% and 97%) as having a lustrous appearance, at least to some degree. On the other hand, one subject (S4) perceived only about 50% of the stimuli as lustrous at all. As expected, the percentage of stimuli perceived as non-lustrous was higher for stimuli with a lower DCD between the center patches.

As we have seen, the sensitivity to perceive binocular luster with chromatic stimuli also strongly depends on the color condition: Half of our subjects (S1, S2, and S3) showed a preference to stimuli in the blue–yellow direction, as indicated by both significantly higher luster settings compared with the RG color condition and lower proportions of non-lustrous judgments (suggesting a lower absolute threshold for luster in the BY stimulus category). The other half of the subjects (S4, S5, and S6) showed the reversed trend—that is, a preference for luster stimuli in the red–green direction.

Discussion

The similarity between the luster curves in the present study and the corresponding curves in our previous study (Wendt & Faul, 2022a) (Figure 2) indicate that the phenomenon of binocular luster in the chromatic case is based on similar mechanisms as in the achromatic case. In particular, interocular contrast pairings with reversed polarities seem to produce considerably stronger lustrous responses compared to pairings with equal polarities. According to our previous approach, this suggests the involvement of (a) different types of monocular cells that are sensitive to chromatic contrasts and respond to different polarities, and (b) a binocular mechanism in which pairs of such monocular signals are integrated with different weights, depending on the between-eye combination of chromatic contrast polarities. This should be reflected in the respective parameters of our chromatic model (see the Model Fit section). That is, we expect interocular contrast pairings with opposite signs to have much stronger weights than interocular pairings with equal signs. However, significant differences in the model parameters between subjects are to be expected also, as the luster curves show some noticeable interindividual difference—for example, with respect to the relative distance between the peak and the baseline level of the lustrous response (especially in the two Consistent conditions) and also between the two different color conditions. Particularly with regard to the perceived strength of the luster phenomenon, the variability among the subjects proved to be much higher for chromatic stimuli than for achromatic stimuli. As an example, taking the peak values for the interocular

luminance difference of the match in the Consistent conditions in both the present and our previous study as a reference, a range between 15 and 25 cd/m^2 can be found in the achromatic case (see Figure 4 in Wendt & Faul, 2022a). In the present study with chromatic stimuli, at least half of our subjects (S1, S2, and S5) barely reached the lower limit of this range at 15 cd/m^2. However, the settings of subject S3 in particular significantly exceeded this range, with peak values of around 38 cd/m^2. Our finding that, on average, there is no difference between the magnitudes of lustrous responses to chromatic and achromatic stimuli—in contrast to previous reports—could therefore be due to the specific composition of the sample, which was small (between five and six subjects) in both studies and therefore not representative. Large differences between subjects regarding the detection threshold for binocular luster were also found in an earlier study with both chromatic and achromatic stimuli (Wendt & Faul, 2019), where the individual proportions of stimuli that were judged as lustrous varied between 8% and more than 95% (Wendt & Faul, 2022b).

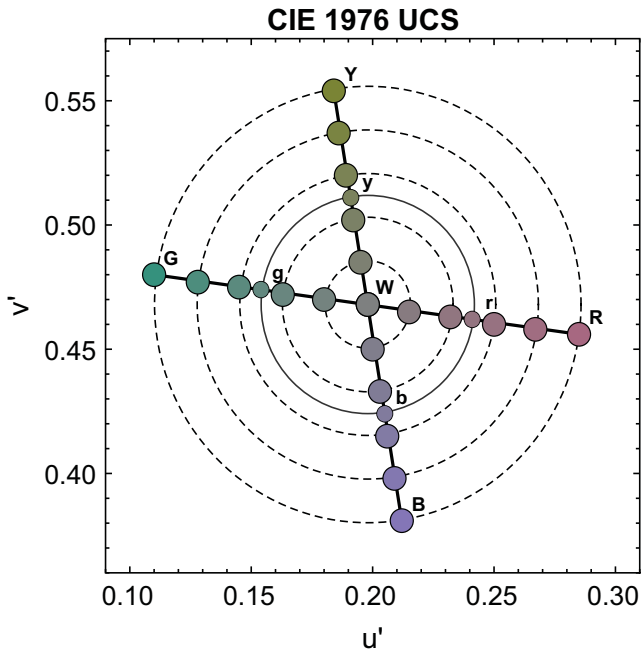

Figure 6. The coordinates of the 11 chromaticities for the ring and the surround element for each of the two color conditions RG and BY as they were used in Experiment 2 (larger disks). The center patch pairs had a dichoptic color difference of 0.5 relative units (r–g and b–y; see the solid circle).

Experiment 2

Using an approach similar to that of the fourth experiment of our previous study (Wendt & Faul, 2022a), we also measured the perceived strength of binocular luster under systematic variation of the chromaticities of the ring and the surround. In this case, the center-ring-surround configurations had a fixed ring width of 0.125 dva and a fixed pair of center patch chromaticities that were set to a relative color distance of 0.5 (see the locations of the smaller disks in Figure 6). For each of the two color conditions, RG and BY, we used 11 chromaticities for both the ring and the surround which were located on the respective line segments in equal steps of 0.2 relative color units (see larger disks in Figure 6). The 11 ring color conditions and 11 surround color conditions were completely crossed with each other. Each of the 121 condition combinations was measured eight times, and the resulting set of 1936 test stimuli (2 color conditions × 11 ring colors × 11 surround colors × 8 repetitions) was presented in random order.

Results

Figure 7a shows the results of Experiment 2 for the averaged data; Figure B1 in Appendix B additionally shows the results for all five subjects (rows). In the top half of the panel, the rating and matching results for color condition RG are shown; in the bottom half, those for the BY color condition (again, the rating and matching values were highly correlated, with correlation coefficients for the individual datasets ranging between 0.924 and 0.969 for the RG condition and 0.856 and 0.987 for the BY condition). Each diagram shows the data as a heat map, where the respective dependent variable is represented as a color value from a dark blue (no luster) to bright yellow (strong luster) continuum, depending on the chromaticity of the ring and surround element of the stimulus. The horizontal and vertical red lines show the chromaticities of the two center patches and subdivide each plot into nine subareas representing different combinations of interocular contrast polarity conditions (Figure 7b). The center area, for example, represents stimulus conditions in which the two center patches had reversed contrast polarities with regard to both the ring and the surround element (Figure 7b, yellow region).

Generally, the strongest luster judgments were observed under these stimulus conditions (only subject S3, again, showed a less systematic result pattern in this regard, at least in the RG color condition; see Figure B1). The weakest luster judgments were found under stimulus conditions in which the center patches were either both incremental (bottom left area in the diagrams) or both decremental to the ring and the surround element (top right area) (Figure 7b, gray regions). Compared to this case, the lustrous responses were considerably stronger when the center patches

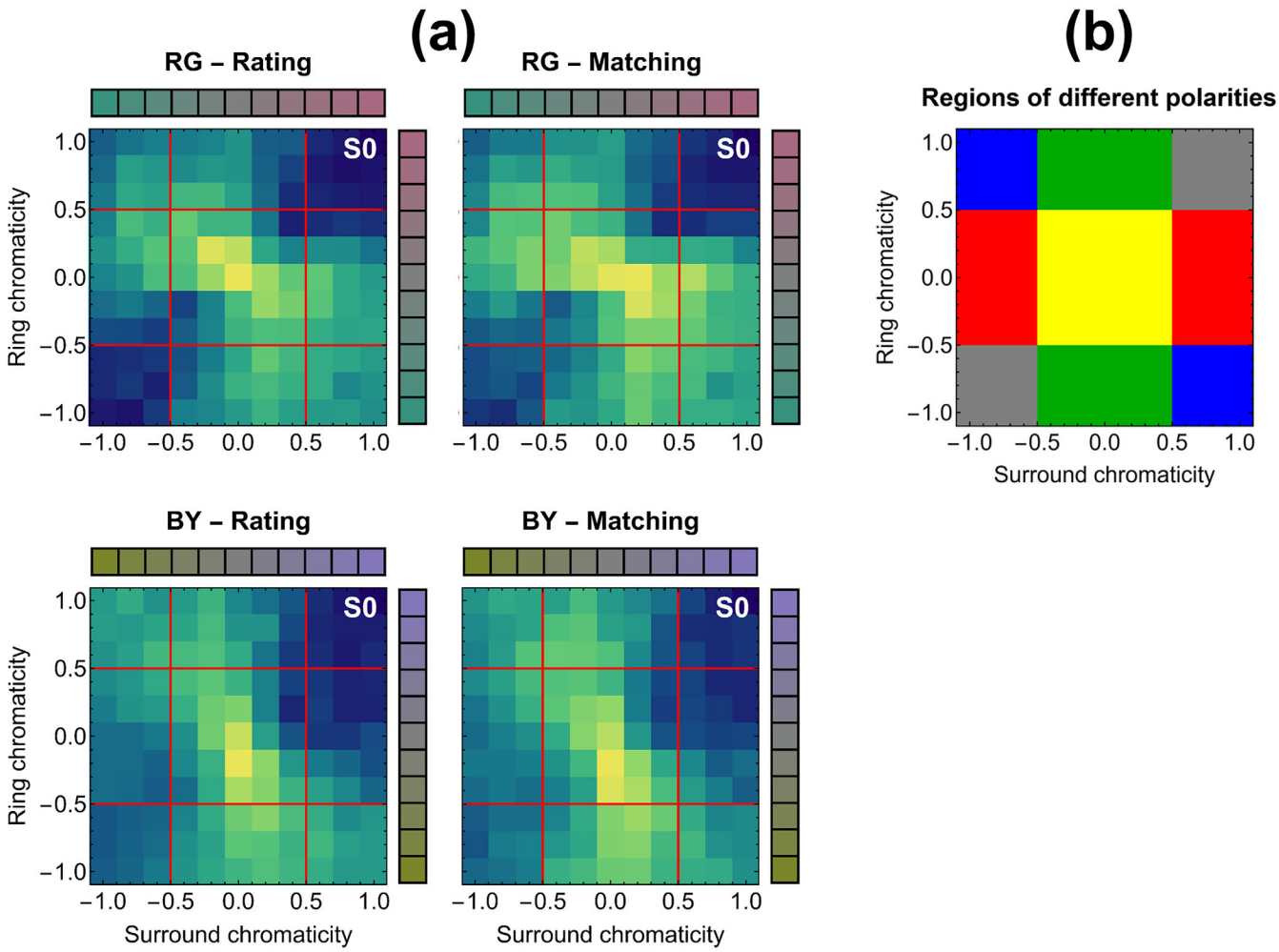

Figure 7. (**a**) Results of Experiment 2 for the data averaged across all subjects (S0). The top pair of diagrams show the results of the rating and the matching task, respectively, for the RG color condition; the bottom pair, those of the BY color condition. In each diagram, the respective dependent variable is plotted as a color value on a continuum of dark blue (no luster) to light yellow (strong luster), in dependence on the surround and the ring chromaticity. The red lines indicate the locations of the chromaticities of the two center patches. See text for further details. (**b**) The chromaticities of the two center patches (red lines in part a) subdivide the diagrams into nine regions characterized by different combinations of interocular contrast polarity conditions: In the yellow area, the two center patches have reversed contrast polarities with regard to both the ring and surround color. In the gray regions, the center patches are either incremental (bottom left region) or decremental (top right region) to the ring and the surround color. The blue regions represent contrast conditions where the center patches are incremental to one stimulus element (that is, either the ring or the surround color) and at the same time decremental to the other stimulus element. The remaining regions show contrast conditions in which the center patches have reversed polarities to one stimulus element—that is, either the ring (red) or the surround (green)—but at the same time consistent polarities to the other element.

were incremental to one stimulus element (ring or surround) and at the same time decremental to the other (which represent stimulus conditions of the Consistent category with a small ring; see Experiment 1) (Figure 7b, blue regions). These as well as the remaining results, where the center patches had reversed contrast polarities to one stimulus element but consistent polarities to the other, are completely in line with our previous findings with achromatic stimuli (Wendt & Faul, 2022a).

Regarding individual color preferences, we found the same trend as in Experiment 1 if only the percentage of stimuli judged as non-lustrous is considered. In Table 2, partial results of a three-way ANOVA (color condition × surround chromaticity × ring chromaticity) are shown for all matching datasets, again with a focus on effects due to the color condition. With respect to the proportion of non-lustrous judgments, subjects S1 to S3 showed a considerably higher sensitivity to luster stimuli from the BY category compared to those from

	Color condition			Non-lustrous (%)	
Subject	RG	BY	*p*	RG	BY
S1	9.25	8.05	<0.001	22.93	7.75
S2	12.36	10.01	<0.001	18.49	2.38
S3	20.38	17.36	<0.001	34.40	1.45
S4	8.72	10.31	<0.001	55.16	65.39
S5	8.14	11.62	<0.001	1.24	47.11
S0	**11.47**	**12.07**	**<0.001**	**26.45**	**24.81**

Table 2. Results of a three-way ANOVA of the matching data from Experiment 2, for both the individual data sets (S1–S5) and the pooled data (S0). Only those results relating to the influence of the color condition on the settings are shown (columns 2–4). Columns 5 and 6 show the proportion of the non-lustrous judgments separately for the two color conditions.

the RG color direction, whereas for the remaining subjects (S4 and S5) this trend was reversed.

However, regarding the strength of perceived luster, there is an unexpected trend that is opposite that observed in Experiment 1. On average, the settings were higher for those stimuli belonging to the color direction with the higher proportion of non-lustrous classifications. That is, although the absolute threshold for luster in a certain color category was comparatively high, suprathreshold stimuli of the same color category produced comparatively stronger sensations of luster.

Discussion

The results of the second experiment are also in good agreement with those of our former study (Wendt & Faul, 2022a). As in our first experiment, a strong dependence of the lustrous impression on the interocular pairing of polarities was found, indicating once again the involvement of different types of chromatic contrast detector cells at the monocular level and a binocular mechanism in which different combinations of these monocular signals are integrated with different weights.

Test of a chromatic version of the interocular conflict model

The results of both experiments suggest similar mechanisms underlying the phenomenon of binocular luster in the chromatic case as we assume for the achromatic case. It can therefore be expected that our interocular conflict model (Wendt & Faul, 2022a) is also suitable for approximately predicting the lustrous responses of the present experiments. Before performing a model fit based on our empirical data, we first describe the chromatic version of our model in detail, in particular the modifications that had to be made to the original achromatic model.

Model description

The latest version of our interocular conflict model for achromatic stimuli (Wendt & Faul, 2022a) consists of three stages (see also Figure 8). In the *first stage*, representing the monocular level, contrast detector cells scan the area of the target region in the two retinal images. In our original achromatic model (Wendt & Faul, 2020), these contrast detector cells were simulated using a Laplacian of Gaussian (LoG) filter kernel, representing the behavior of the retinal ON-center and OFF-center cells that exhibit an antagonistic, circular-symmetric center-surround receptive field. We later found that our achromatic model works equally well (that is, without substantial loss of predictive power) when a Gabor filter kernel is used instead of LoG filters (Wendt & Faul, 2022a).

In our achromatic model, this Gabor filter kernel represents cells in V1 that were found to have receptive fields in which the antagonistic regions are spatially arranged side by side, where a central excitatory part is flanked by inhibitory parts at both sides, or vice versa (see Figures 9c and Figure 9d, respectively). This cell type for the monocular stage of the achromatic model is more consistent with the assumption of Kingdom and colleagues (2022) that the binocular stage, in which the two monocular signals are integrated, is represented by so-called tuned-inhibitory cells, which presumably receive their inputs from such monocular cells (see also the General Discussion section).

For the chromatic version of our model, there also appear to be several candidates for monocular cells that respond to chromatic contrasts. Evidence for such cells has been found, for example, in single-unit recordings in the V1 area of primates (Conway & Livingstone, 2006; Johnson, Hawken, & Shapley, 2001; Schluppeck & Engel, 2002). Based on the data obtained in these studies, models of the structure of the receptive fields of these cells were developed. These cells are referred to as double-opponent cells, because their receptive fields combine two types of opponency (Conway, 2009; Gegenfurtner, 2003; Horwitz, 2020; Solomon & Lennie, 2007): (a) opponency with respect to cone excitations, in which signals from different cone types are antagonistically integrated, and (b) spatial opponency, in which different spatial areas of the receptive field are antagonistic to each other.

The cone opponency is comparatively well understood: The L-cone and M-cone represent one type of cone opponency (L–M or –L+M) and the S-cone and a combination of the L- and M-cones a second type (S–[L+M] or –S+[L+M])

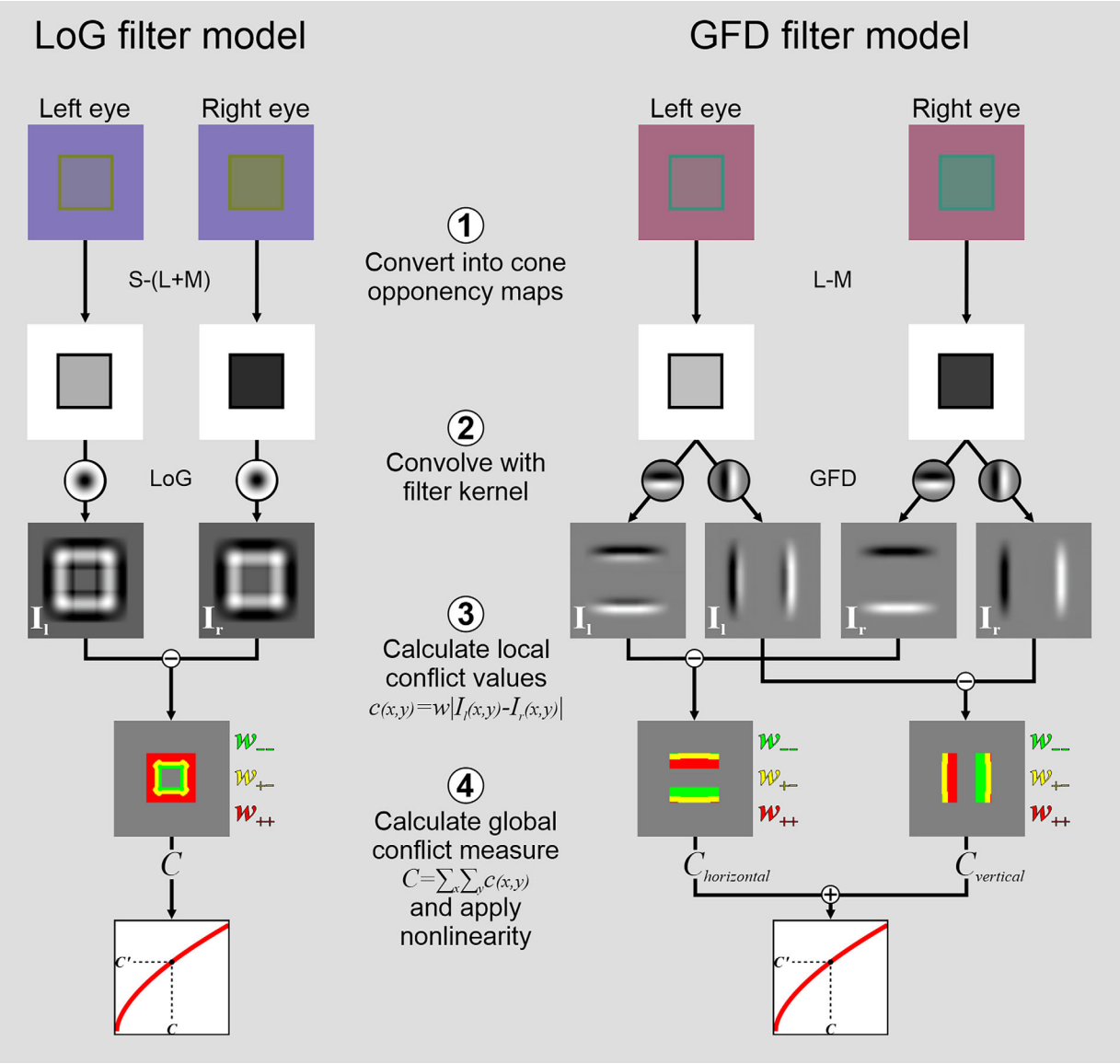

Figure 8. Schematic representation of the chromatic version of the interocular conflict model, separately for the LoG (left) and the Gaussian first derivative (GFD) (right) filter models. For the LoG model, the Consistent A stimulus of the BY color condition is used as an example; for the GFD model, the Consistent A stimulus of the RG color condition is used. In the first step, the two half-images of a dichoptic stimulus pair are converted into maps representing cone opponency. In step two, these maps are convolved with the respective filter kernel. In the GFD model, this was separately done with a horizontally and a vertically oriented filter kernel. In the third step, the resulting images, I_l and I_r, were used to calculate local conflict values, $c(x,y)$. This was done for each corresponding pixel pair within the target area. The local measure is the absolute difference of corresponding filter values, weighted by w, which depended on the signs of the two filter values (red, green, and yellow regions represent these three different types of interocular polarity combinations). Note that, in the GFD model, the weights for pairings with same signs (w_{++} and w_{--}) were equal. The sum of the local conflict values represents the global conflict measure C to which a nonlinear transducer was applied (step 4). See the main text for further details.

(Conway & Livingstone, 2006). Note that there are alternative ways to combine the cone excitations. For example, to account for neurophysiological data provided by Johnson et al. (2001), Johnson, Hawken, and Shapley (2008), Wang and Spratling (2016) weighted the M-cone excitations by a factor of 0.8 when combining them with the L-cone excitations in their receptive field model. In the other type of cone opponency, the S-cone excitations are sometimes combined with the mean of the L- and M-cone excitations, leading to S–(L+M)/2 instead of S–(L+M). However, we found that our chromatic model is very robust to different methods for calculating cone opponency: The main parameters of this model—that

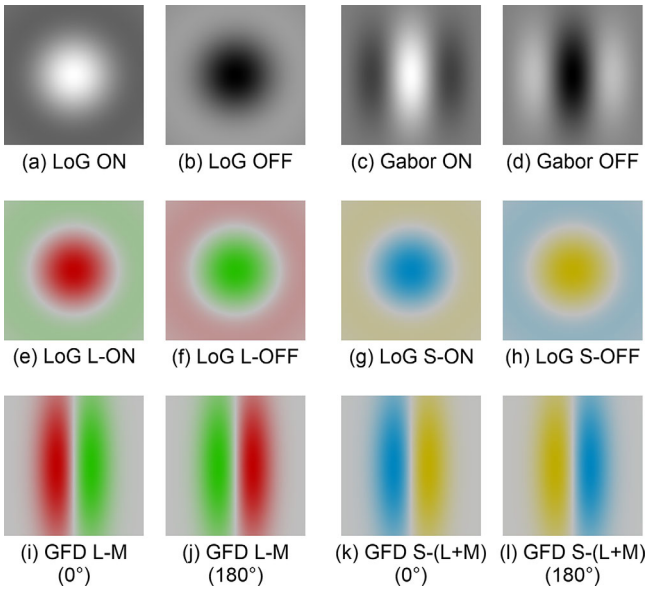

Figure 9. Schematic representation of different receptive field models based on different filter kernels. (**a**, **b**) ON- and OFF-center cells (such as the retinal ganglion cells), respectively, with an antagonistic center-surround organization (light pixels represent excitatory areas, dark pixels inhibitory areas). (**c**, **d**) Orientation-selective ON- and OFF-center cells based on a Gabor filter kernel. Our data obtained with achromatic stimuli could be predicted equally well with both filter pairs (Wendt & Faul, 2022a). (**e**–**h**) Color-sensitive receptive fields with a circular-symmetric structure of spatial opponency. For example, L-ON-center cells are responsive to light patterns that stimulate L-cones in the central area more than in the surround area. Accordingly, L-OFF-center cells are triggered by light patterns that produce stronger L-cone excitations in the surround area than in the center. (**i**, **j**) Receptive fields of orientation-selective cells responsive to differences between the L- and the M-cone excitations, in which the antagonistic parts are arranged side by side and which are based on the GFD. These double-opponent cells are orientation selective and are shown here with opposite orientations. (**k**, **l**) Receptive fields with the same type of spatial opponency that are responsive to differences in the S-cone excitations.

is, the weights for the different types of interocular polarity pairings (see below), as well as the size of the filter kernel—are completely unaffected by this factor. The predictive power of the model also varies at most in the per-mille range due to these changes. Only the scaling factor of the nonlinearity (see below) is influenced to some larger extent.

With regard to spatial opponency, however, different receptive field models are discussed (De & Horwitz, 2021; Johnson et al., 2008; Shapley & Hawken, 2002; Shapley & Hawken, 2011; Solomon & Lennie, 2007). This includes both circular-symmetric center-surround layouts (similar to those of the retinal ganglion cells) and orientation-selective receptive fields, in which the antagonistic parts are located side by side. Here, we consider both types in order to test which one is more compatible with our data.

We used strongly idealized receptive field models in our chromatic model (e.g., Lindeberg, 2013; Lindeberg, 2021; Wang & Spratling, 2016). Both half-images of our dichoptic stimuli were convolved with two different filter kernels representing the two different types of spatial opponency of the monocular cells' receptive fields (step 2 in Figure 8). In one version of our chromatic model, an LoG filter kernel was used to model receptive fields with an antagonistic circular-symmetric center-surround structure (Figures 9e through 9h). In another version, a kernel based on the first derivative of a Gaussian was used, which represents the receptive field type with a side-by-side arrangement of the antagonistic parts (see Figures 9i through 9l). This alternative receptive field model, which we also refer to as the Gaussian first derivative (GFD) filter, is based on data from single-unit recordings in the primary visual cortex of macaques (Johnson et al., 2008; Lindeberg, 2021). The convolution with the filter kernel, however, is not performed on the original images whose colors are defined by their u′,v′,L values (see the Stimulus section), but rather, in order to account for cone opponency, on images whose pixels represent the respective combination of different cone excitations. That is, the u′,v′,L images were first converted to LMS coordinates (based on Stockman & Sharpe, 2000) and then converted into maps whose pixel values represent either L–M (for stimuli of the RG color condition) or S–(L+M) (for stimuli that belong to the BY color condition; see step 1 in Figure 8). As in our previous study, the optimal size of the respective filter kernel is determined empirically when the model parameters are fitted with the experimental data.

After the convolution with the filter kernel, the pixels of the resulting images I_l and I_r will have a positive or a negative sign (or a value of 0; note that, in order to account for rounding errors, unsigned filter values below a threshold of 10^{-6} were taken as 0). This sign of the filter value determines what kind of double-opponent cell (in each color category) was stimulated at a given position. In the case of the circular-symmetric receptive field, it indicates whether an ON- or OFF-center mechanism was triggered by the stimulus (see Figure 8). A negative pixel value of the LoG-filtered image in the RG condition, for example, would represent the stimulation of a cell with an L+M– center area of its receptive field and an M+L– surround (which we will also refer to as L-ON cell; see Figure 9e), whereas a positive value represents the stimulation of a cell with an M+L– center and an L+M– surround area of the receptive field (L-OFF cell; see Figure 9f). For the orientation-selective receptive field type, in which the antagonistic parts are arranged side-by-side, the ON-/OFF-center dichotomy does not make any sense, as there is no central part. In this case, the different signs in the filtered image represent

receptive fields with opposite orientations (Figure 9, bottom row). Note that, in the case of this receptive field type, each stimulus image (with square center and ring elements) will be convolved with both horizontally and vertically oriented GFD filter kernels (see step 2 of the GFD filter model in Figure 8). For the convolution with the LoG filter, we used the Mathematica function LaplacianGaussianFilter with variable radius r_{LoG} of the kernel, where the width of the Gaussian equals $r_{LoG}/2$. For the convolution with GFD filters, we used the Mathematica function GaussianFilter, also with variable radius r_{GFD}, where the original width of the Gaussian ($r_{GFD}/2$) in one direction was scaled with factor 0.5 and in the other direction with a factor of 1.5 (cf. Lindeberg, 2021) (Figure 9, bottom row).

In the *second stage* of our model, representing the binocular level at which the two monocular signals are combined into a local conflict value, the signs of the monocular signals play an important role. For cell types that can be described by means of an ON-/OFF-center dichotomy, we showed in our previous study that different between-eye combinations of ON- and OFF-center mechanisms contribute with different weights to the overall conflict measure. The binocular pairing of an ON-center and an OFF-center mechanism was found to produce considerably stronger conflict values compared to ON–ON or OFF–OFF pairings, a finding that is in good agreement with the observation that inc–dec stimulus configurations elicit much stronger sensations of luster than inc–inc or dec–dec configurations (which would exclusively produce ON–ON and OFF–OFF pairings, respectively) (Figure 1). In order to determine the weights for the three different interocular contrast polarity combinations, we performed grid searches separately for the two types of cone opponency (or color conditions). Because only relative weights matter for the calculation of the conflict measure, the weight for the ON–OFF pairing was set to a value of 1.

For the other type of receptive field with a side-by-side spatial arrangement of the antagonistic parts, the ON–OFF center dichotomy cannot be applied. Therefore, we only consider the two cases of (a) where the signs of corresponding filter values are equal or (b) where these signs are opposite between eyes. Again, we assume a binocular conflict mechanism in which these two cases are treated differently. Because we expected the latter case with unequal signs (representing the stimulation of double-opponent cells with opposite orientation of their receptive fields) to have a much stronger effect on the lustrous response, its weight was set to 1. The weight in the other case (in which cells with equally oriented receptive fields are stimulated at corresponding locations) was determined empirically to best predict our luster data. We also tested a version of the GFD-based model with three independent weights for the three different interocular combinations of signs of the filtered values (+−, ++, and −−) (Figure 8). However, this distinction between the two cases with equal signs did not improve the prediction, confirming that the use of equal weights for these two cases is justified.

The local conflict value at each pixel position within the target area is calculated in the same way as in the achromatic version of our model—namely, by binocular differencing (Henriksen & Read, 2016; Kingdom, 2012): $w|I_l(x,y) - I_r(x,y)|$; that is, corresponding filter values of the two half-images are subtracted and the result full-wave rectified. This signal is then multiplied with weight w, a parameter that is dependent on the type of interocular contrast polarity pairing (ON–ON, OFF–OFF, or ON–OFF in the case of the LoG filter kernel) or on equal versus reversed filter orientation in the case of the GFD filter kernel (see step 3 in Figure 8).

The *third stage* of our model represents a hypothetical mechanism in which the local conflict values are spatially integrated over the area of the target field to form a global conflict measure C, which determines the overall magnitude of the lustrous response elicited by the given stimulus. In our previous study, we found that a simple summation of the local conflict values works well in this respect. However, the predictions of the empirical luster judgments (L) are further improved when this global conflict measure (C) is adjusted by a nonlinear transducer of the form $L = a^*C^c$ (step 4 in Figure 8). The parameters a and c of the transducer function are also determined based on our empirical data. In our previous study, with achromatic stimuli, these transducer functions were compressive for stronger conflict signals and were similar to those found in a study by Kingdom, Seulami, Jennings, and Georgeson (2019), in which thresholds for the detection of interocular contrast differences were measured. It is possible that further nonlinearities occur at previous stages of the sequence of processing units involved in the phenomenon of binocular luster. We explicitly tested a variant of our chromatic model where an additional nonlinearity was applied to the second stage (on the local conflict signals), but we did not find a significant improvement of the predictions.

Model fit

To determine the weights for the different interocular contrast polarity combinations, we conducted a grid search. This was done separately for the two different filter kernels (representing different types of receptive fields; see the Model section) and the two different color directions (representing different types of cone opponency). In all cases, we used R^2, the coefficient of determination, to assess how well the empirical data,

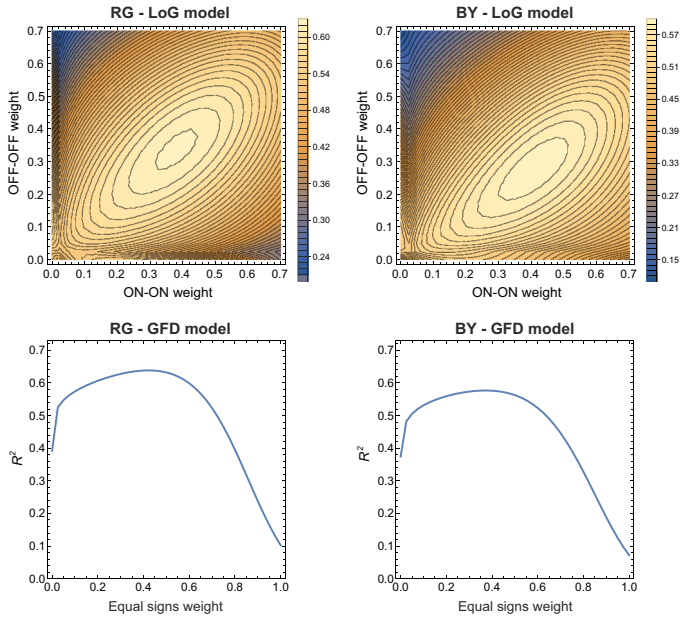

Figure 10. Results of the grid search used to determine the weights for the different types of interocular contrast polarity combinations. They are based on the luster settings averaged across all subjects (S0) from both experiments. In the top row, the results for the LoG model are shown, separately for the RG and the BY color conditions. In both diagrams, the R^2 values are plotted as a function of the combination of the ON–ON and the OFF–OFF weights. In the bottom row, the results for the alternative receptive field model (GFD) are shown, also separately for the RG and the BY color condition. Note that, in this case, we assumed that interocular pairings with equal signs have equal weights. Another parameter that was taken into account in the grid search was the radius of the filter kernel. All diagrams show the respective layer of the radius that produced the highest R^2 values (for details, see the respective S0 rows in Tables 3 and 4).

both for the pooled and the individual datasets, are predicted by our model. Based on the findings of our previous study (Wendt & Faul, 2022a), we assume that the magnitude of the lustrous response is a nonlinear function of the conflict measure C. Therefore, we calculated R^2 for the best fitting parameters a and c of the function $L = a*C^c$ (where L represents the luster setting) while systematically varying the remaining model parameters. In the case of the LoG filter model, these were the radius of the filter kernel as well as the weights for the ON–ON and the OFF–OFF polarity pairings (with the weight for the ON-OFF pairing set to 1.0). In the case of the GFD kernel, the remaining parameters were the radius of the kernel and the weight for the binocular combination in which both monocular filter kernels had the same orientation (equal signs weight), whereas the weight for the binocular pairing with opposite filter kernel orientations was set to 1.0.

Results and discussion

LoG filter model

Figure 10 shows the results of the grid search for the pooled matching data, for both the RG (left) and the BY (right) color condition. The contour plots in the top row show the R^2 value for the LoG filter model as a function of the weights of the ON–ON and OFF–OFF pairings. In both cases, the layer with the optimal filter radius r_{LoG} is shown: $r_{LoG} = 12$ pixels for the RG condition and $r_{LoG} = 20$ pixels for the BY color condition. The peak R^2 values for the averaged data were $R^2 = 0.6227$ for the RG color condition and $R^2 = 0.597$ for the BY color condition. Model parameter values for all datasets are shown in detail in Table 3. The prediction accuracy is slightly worse than for the achromatic case, where an overall R^2 value of 0.818 was found (Wendt & Faul, 2022a). The interindividual differences in the empirical luster judgments are also reflected in the variability of the model parameters (Table 3).

Although, on average, the radius r_{LoG} of the LoG filter kernel in the RG color condition was comparable to that in our previous study with achromatic stimuli ($r_{LoG} = 12$ pixels), this radius varied between 6 and 24 pixels for the individual datasets. The LoG filter radius was generally much higher for the BY color condition (with $r_{LoG} = 20$ pixels for the pooled data and radii for the individual datasets ranging between 8 and 33 pixels), indicating larger receptive fields for the S-ON or S-OFF double-opponent cells compared to those sensitive to the other color direction. The weights for the ON–ON and OFF–OFF pairings also varied considerably among the subjects. However, all of these weights are much lower than the weight for the ON–OFF pairings (which was set to 1.0; see the model description), indicating that conflict signals based on equal polarities contribute much less to the overall conflict measure than signals with different polarities.

The goodness of the model fit (R^2) differed significantly among individual datasets, with especially low values for subject S3, who occasionally showed some rather unsystematic data trends (particularly in the BY color condition). In contrast, the R^2 values for subject S6 are extraordinarily high ($R^2 > 0.81$), which is at least to some extent due to the fact that this subject only participated in Experiment 1. Generally, for currently unknown reasons, model predictions were better for the data obtained in Experiment 1 than for the data of Experiment 2. This can be seen in Figure 11, where the mean luster settings are plotted against corresponding conflict measures C (data points belonging to Experiment 1 are shown as red and those belonging to Experiment 2 are shown as green dots in the diagrams). For the color condition BY, the relationship between the mean luster settings and

Subject	ON–ON Weight	OFF–OFF Weight	r_{LoG}	a	c	R^2
RG Color Condition						
S1	0.200	0.100	24	1.1284	0.6558	0.6364
S2	0.250	0.525	10	0.1924	0.9406	0.5356
S3	0.725	0.025	6	1.4824	0.5242	0.4843
S4	0.150	0.250	10	0.0531	1.2961	0.5171
S5	0.525	0.525	21	0.9734	0.7105	0.6485
S6	0.000	0.100	16	8.8148	0.2838	0.8928
S0	**0.375**	**0.325**	**12**	**0.3807**	**0.8604**	**0.6227**
S0 linear	**0.425**	**0.375**	**12**	**0.2055**	**1.0000**	**0.6197**
BY Color Condition						
S1	0.075	0.025	23	2.3602	0.3022	0.6770
S2	0.500	0.275	33	0.9795	0.5404	0.5297
S3	0.425	0.000	8	10.4206	0.1339	0.1319
S4	0.075	0.025	18	0.0106	1.1931	0.4931
S5	0.475	0.325	31	0.0062	1.3230	0.6035
S6	0.000	0.150	17	2.1235	0.3966	0.8123
S0	**0.400**	**0.275**	**20**	**0.4091**	**0.6175**	**0.5970**
S0 linear	**0.550**	**0.450**	**18**	**0.0368**	**1.0000**	**0.5595**

Table 3. Parameter values for the model based on the LoG filter kernel for all subjects (S1–S6) and the pooled data (S0). In the top half, the values for the RG color condition are shown; in the bottom half, those for the BY color condition are shown. The last row in each subtable shows parameter values for an alternative model with a linear transducer based on the pooled data (S0 linear).

the conflict measures calculated by our model can be described by a decelerating power function (with exponent $c < 1.0$), which is also in agreement with our previous findings (Wendt & Faul, 2022a). However, this relationship is nearly linear for the other color condition, RG (Figure 11). But, also regarding the shape of the fitting curve, there were large differences among subjects. For the pooled data, we also tested a version of our model with a linear transducer for the global conflict measure C in the form $a*C$ (i.e., without an additive constant). As can be seen in the corresponding rows of Table 3 (S0 linear), this has some impact on the model parameters. However, predictability was not greatly reduced (with R^2 values of 0.6197 and 0.5595 for the RG and the BY color conditions, respectively), suggesting that a linear transducer would also be generally compatible with our chromatic model. Note that better predictions (with $R^2 = 0.6222$ in the RG condition and $R^2 = 0.6143$ in the BY condition) were obtained when a linear model with an additive constant was used. We already found a strong linear relationship between luster judgments and model predictions with our original model for achromatic stimuli based only on conflicts due to interocular ON–OFF pairings (with R^2 values up to 0.84) (Wendt & Faul, 2020). However, the positive y-intercept of the linear regression was difficult to interpret in terms of an interocular conflict mechanism, as it meant that luster was perceived to a significant degree even in stimuli for which the model predicted no conflict at all. The zero point is therefore an essential component of our model, which eventually motivated our improved version with additional parameters and the use of a nonlinear transducer function.

To facilitate comparison between the empirical luster settings and the corresponding model predictions, they are shown together in Figure 12 (for Experiment 1; see the top panel for the LoG model) and Figure 13 (for Experiment 2), using the matching data averaged across all subjects. Although the absolute values differ somewhat between the mean luster settings and their predictions, the general trends are very similar, particularly with respect to the data of Experiment 1 (compare corresponding black and red curves in the diagrams of Figure 12). This is also true for the data of Experiment 2 (Figure 13), although the range of the predicted values is somewhat lower compared to the range of the empirical luster settings: That is, the strongest sensations of luster are produced by stimuli where both center patches show reversed contrast polarities between eyes to both the ring and the surround element (center area in the diagrams), whereas the weakest lustrous responses occur in stimuli where both center patches have the same consistent contrast polarities regarding the ring and the surround element (bottom left and top right area in the diagrams). For the remaining interocular contrast polarity combinations, the lustrous responses are somewhere in between, which is also in agreement with the empirical data.

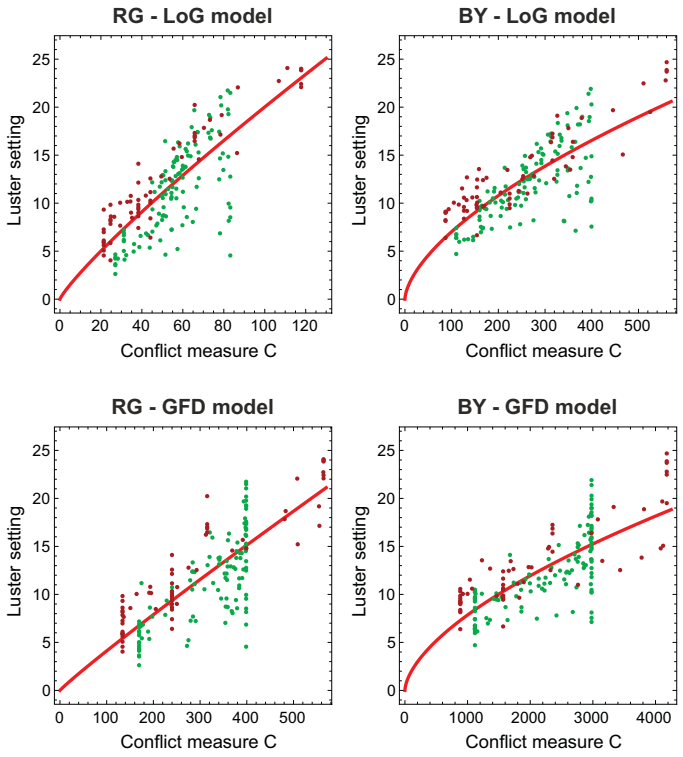

Figure 11. The diagrams show the relationship between the empirical luster settings (based on the pooled matching data) and corresponding conflict measures *C*, separately for the two different receptive field models (rows) and the two color conditions RG and BY (columns). In the diagrams, the data from Experiment 1 are shown as red dots and those of Experiment 2 as green dots. In each case, *C* is based on the optimal filter radius and the optimal weights for the different interocular contrast polarity pairings, as they were determined in the grid search (see also Figure 10 and Tables 3 and 4 for details). The red curves show the fit with a power function.

GFD filter model

A very similar picture emerges with respect to the alternative filter model based on the first derivative of a Gaussian. The bottom row in Figure 10 presents the results of the grid search for the GFD filter kernel for both the RG (left) and the BY (right) color direction. Each diagram shows R^2 as a function of the weight for equally oriented filter pairs, again for the optimal filter radius r_{GFD}. For the RG color direction, the optimal filter size was $r_{GFD} = 22$ pixels; for the BY color direction, it was $r_{GFD} = 35$ pixels. The peak R^2 values for the RG and the BY color directions computed for the pooled data ($R^2 = 0.6387$ and $R^2 = 0.577$, respectively) are very similar to the corresponding values of the LoG filter model. The model parameters estimated separately for the individual datasets varied considerably (Table 4). Overall, the trends in the data are similar to those found with the LoG filter model: The prediction was somewhat better for the RG color condition, the size of the filter was larger for the BY condition, and the weight for the pairs with equally oriented filter kernels was considerably lower than for pairs with opposite filter orientations (which was set to a value of 1.0). In the bottom part of Figure 11, the mean luster settings averaged across all subjects are plotted against corresponding conflict measures *C*. Again, a nonlinear relationship between these two measures was found for the BY condition (indicated by the red fitting curve) and a nearly linear relationship for the RG color condition. However, using a linear transducer (without an additive constant; see above) in both cases would not severely impair the predictive power of our model (see the corresponding S0 linear rows in Table 4).

The bottom rows of Figure 12 (Experiment 1) and Figure 13 (Experiment 2) show a direct comparison between the empirical data and the corresponding model predictions of the GFD filter model. As with the LoG model, the data of the first experiment could be rather well predicted. The predictions for the second experiment show similar problems as with the LoG model: Although the general trends regarding the influence of the interocular contrast polarity combinations on the lustrous sensation are well preserved, the model has difficulty reproducing the full range of luster values observed in the experiment.

General discussion

The main aim of the current study was to investigate whether the phenomenon of binocular luster in the chromatic case can be described with a model similar to the one we proposed for the achromatic case (Wendt & Faul, 2022a). We essentially repeated the experiments of our earlier investigations with chromatic stimuli and extended the model for achromatic stimuli analogously to the chromatic case.

The results of the two experiments, as well as the test of the chromatic model, provide strong evidence that the mechanisms underlying the phenomenon of binocular luster share the same features in both the chromatic and the achromatic cases. This mechanism is highly sensitive to interocular pairs of contrasts with reversed polarities and significantly less responsive to contrasts with equal signs. Although our results indicate that at the monocular stage different types of contrast detector cells are involved, which are sensitive to different contrast polarities, the exact properties of these cells are still unclear. Our results show that the data are compatible with different receptive field types. This is true not only for the present study but also for the achromatic case. In each case, we found that different receptive field models make similar predictions, making both equally suitable to serve as monocular contrast detectors contributing to binocular luster.

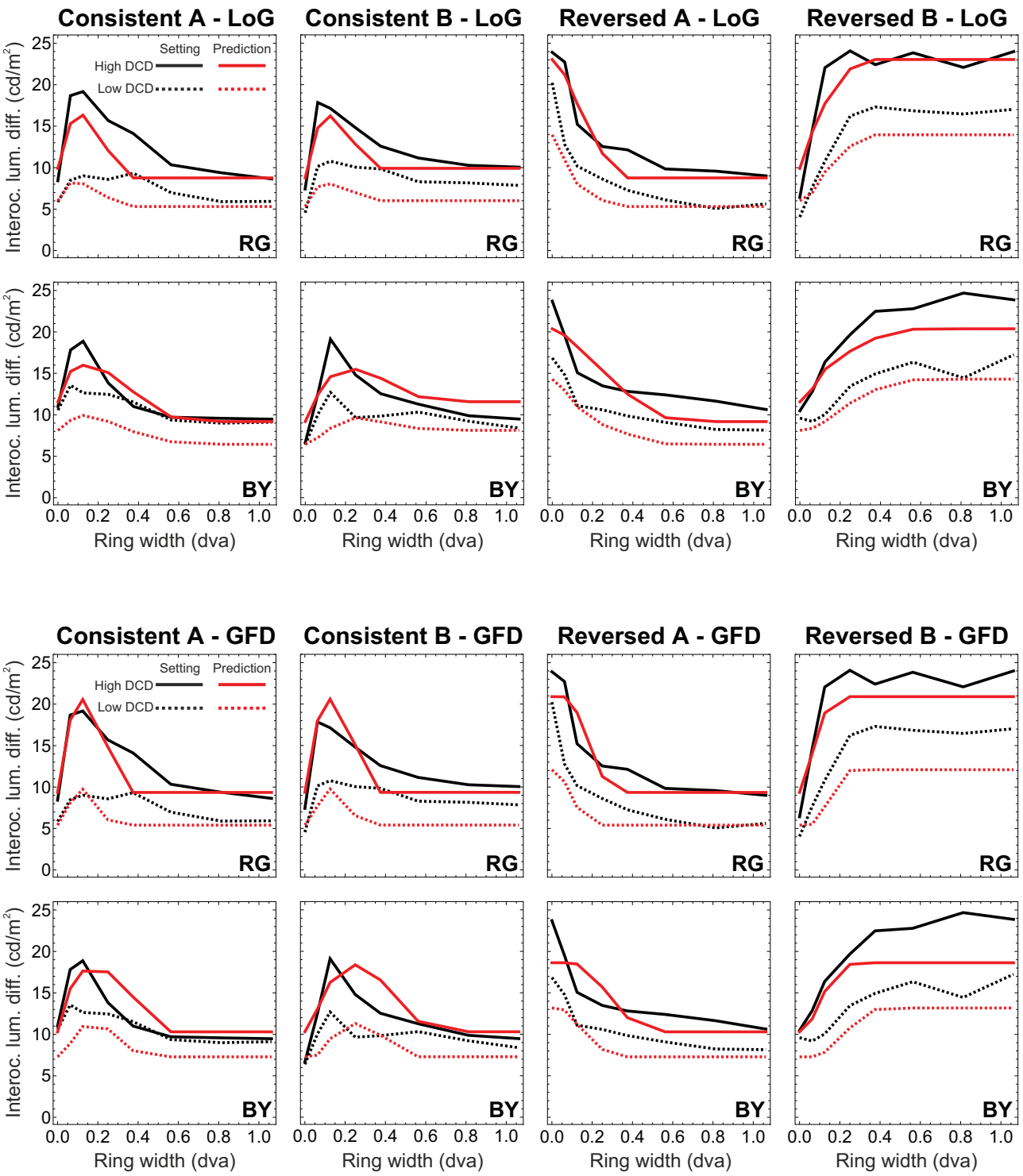

Figure 12. Direct comparison between the empirical luster settings and their predictions with our model. The averaged data (S0) of Experiment 1 (black lines) are shown together with their corresponding predictions (red lines), separately for the two different receptive field models (upper and lower panels) and the two different color conditions (RG in the top row of a panel, BY in the bottom row). The conditions with a higher dichoptic color difference between center patches (high DCD) are shown as solid lines, those with a lower DCD as dotted lines. Note that for the calculation of the prediction values, the conflict measure *C* was adjusted by taking the respective nonlinearity into account (see the respective parameters *a* and *c* in Tables 3 and 4).

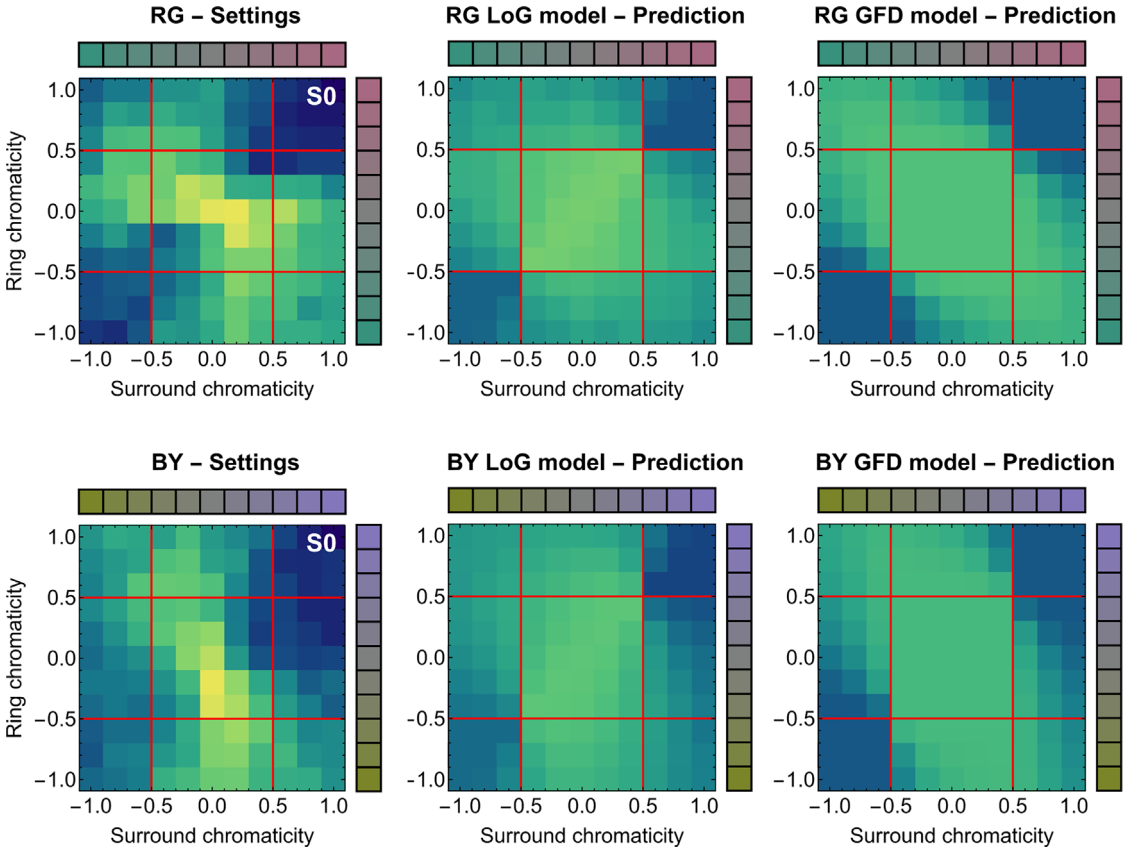

Figure 13. Direct comparison between the empirical luster settings and their predictions with our model. Averaged data (S0) of Experiment 2 (left column) are shown together with their corresponding predictions, separately for the two different receptive field models (middle and right columns) and the two different color conditions (rows). Note that, for the calculation of the prediction values, the conflict measure *C* was adjusted by taking the respective nonlinearity into account (see the respective parameters *a* and *c* in Tables 3 and 4).

Subject	Equal signs weight	r_{GFD}	*a*	*c*	R^2
RG Color Condition					
S1	0.100	39	0.3944	0.5755	0.6820
S2	0.475	16	0.0455	0.9363	0.4388
S3	0.075	15	1.9500	0.3997	0.3753
S4	0.250	26	0.0022	1.5020	0.4791
S5	0.575	45	0.3695	0.6240	0.5531
S6	0.150	28	0.0542	0.3307	0.8138
S0	**0.425**	**22**	**0.0542**	**0.9399**	**0.6387**
S0 linear	**0.450**	**20**	**0.0371**	**1.0000**	**0.6380**
BY Color Condition					
S1	0.100	37	0.8529	0.3404	0.6548
S2	0.400	50	0.3407	0.4999	0.4442
S3	0.075	13	14.8448	0.0686	0.1498
S4	0.250	30	<0.0001	1.9326	0.5618
S5	0.400	50	0.0008	1.1692	0.5322
S6	0.200	27	0.9916	0.3840	0.7046
S0	**0.375**	**35**	**0.1209**	**0.6042**	**0.5770**
S0 linear	**0.550**	**33**	**0.0049**	**1.0000**	**0.5313**

Table 4. Parameter values for the model based on the GFD filter kernel for all subjects (S1–S6) and the pooled data (S0). In the top half, the values for the RG color condition are shown; in the bottom half, those for the BY color condition are shown. The last row in each subtable (S0 linear) also shows, based on the pooled data, corresponding parameter values for our model with a linear transducer.

A similar statement can be made with respect to the second stage of our model, representing binocular cells that respond to interocular conflicts in the form of contrast differences between eyes, especially contrasts with reversed polarities. Also in this case, additional evidence from neurophysiological studies is needed. For the achromatic case, Kingdom and colleagues (2022) proposed that so-called *tuned-inhibitory cells* provide the physiological basis for the phenomenon of binocular luster. In studies in which single-unit recordings were obtained from the V1 area of macaques, this binocular cell type was found to respond strongly to anti-correlated random dot stereograms (RDSs) when these stimuli were presented with zero disparity, but only weakly when correlated RDSs were used (Prince, Cumming, & Parker, 2002; Read & Cumming, 2003; Read & Cumming, 2004).

This is in agreement with findings from psychophysical studies that the lustrous response is considerably stronger in stimuli with reversed contrast polarities compared to stimuli with consistent contrast polarities between eyes (Anstis, 2000; Georgeson et al., 2016; Wendt & Faul, 2019; Wendt & Faul, 2020; Wendt & Faul, 2022a) (Figure 1). In our model, this observation is captured by using different weights for different interocular contrast polarity combinations. However, rather than being a specific detector for binocular luster, the tuned-inhibitory cells are assumed to be a part of a mechanism aimed at solving the stereo correspondence problem and thus enabling stereopsis. It is hypothesized that the tuned-inhibitory cells complement a family of other binocular cell types involved in stereopsis and act as a kind of "lie detector" that detects non-matching luminance patterns between the retinal images (Goncalves & Welchman, 2017; Read & Cumming, 2007).

Because we assume similar mechanisms in both the chromatic and achromatic case of binocular luster, this raises the question of whether similar binocular neurons exist in the color domain which are also involved in the processing of stereo-disparity information. Is it even possible to produce depth sensations with isoluminant stimuli? Early studies using RDSs as stimuli generally deny this (de Weert, 1979; Lu & Fender, 1972). However, later studies were able to show that stereopsis with isoluminant RDS stimuli is indeed possible, provided that further stimulus features are taken into account. Depth sensations were found to occur only within a narrow range of disparities and with much stronger chromatic contrasts compared to corresponding black and white stimuli (Jimenéz, Rubino, Hita, & Jiménez Del Barco, 1997; Kingdom & Simmons, 1996; Simmons & Kingdom, 1994). The size of the stimulus elements also seems to play a role: In the study by de Weert (1979), stereopsis was found to be present in isoluminant stimuli when figural stimuli in the form of vertical bars were used instead of RDSs, indicating that the spatial resolution of the underlying color-sensitive mechanisms is much weaker than in their luminance-based counterparts. However, even under optimal stimulus conditions, performance on visual tasks was generally considerably less precise in the chromatic case than in the achromatic case (which also seems to be true for the phenomenon of binocular luster, as our data suggest). Nevertheless, all of these findings, including ours, are not in conflict with the idea that binocular luster in the chromatic case is mediated by a binocular mechanism similar to that proposed by Kingdom et al. (2022) for the achromatic case.

Additionally, it is also possible that these mechanisms are not only similar but in fact identical. A large population of cells in the V1 area of primates has been found to be responsive to both luminance contrasts and pure chromatic contrasts (at least to contrasts varying in L- and M-cone excitations; see Johnson et al., 2001; Thorell, De Valois, & Albrecht, 1984).

However, a low-level conflict approach generally has the problem of explaining why the detection of interocular contrast differences should be made conscious by the visual system in the first place (and why in the form of a lustrous impression). Is there a functional purpose for this behavior or is binocular luster simply the unintended result of a "neural accident" (Wendt & Faul, 2022a)? Indeed, the stimulus conditions for binocular luster are extremely artificial. In particular, the occurrence of reversed contrast polarities between eyes is unlikely under natural viewing conditions (Read & Cumming, 2007). Thus, it would not be unreasonable to assume that the visual system was never prepared to respond to such stimuli and that binocular luster reveals some kind of neural dysfunction—a dysfunction that can nevertheless give us deeper insights into visual processing.

In contrast, Vladusich, Lucassen, and Cornelissen (2007) assumed that, rather than being the result of a low-level process, the phenomenon of binocular luster arises from the simultaneous perception of brightness and darkness, triggered by incremental and decremental light patterns at corresponding retinal locations, respectively. Their empirical findings suggest that the perception of achromatic colors is inadequately described by a one-dimensional dark–light continuum, but that it requires a two-dimensional space based on darkness and brightness as dimensions. If we extend this approach to the perception of chromatic colors, this could provide a higher level explanation for the occurrence of binocular luster in isoluminant stimuli, especially in cases where chromatic contrasts with reversed polarities are dichoptically combined. The idea that the full variety of color impressions, with their different modes of appearance, cannot be explained with a simple triplet of cone excitations has already been discussed earlier (e.g., Mausfeld & Niederée, 1993; Niederée, 2010).

Future work

In our previous work (Wendt & Faul, 2022a) and in our present study, we investigated interocular variations in luminance and in the two opponent color mechanisms in isolation. However, our findings from both studies now offer the possibility of constructing a general model of binocular luster, based on the L-, M-, and S-cone excitations, which can predict the magnitude of the lustrous response in any arbitrary dichoptic pair of stimuli. The main question would be how the effects of these three different mechanisms are combined. For example, for stimuli that trigger interocular conflicts in more than one of these mechanisms, the lustrous response could be some kind of average or the sum of the individual effects. In an earlier study, we investigated the lustrous effect elicited by simple center-surround stimuli using different color directions (Wendt & Faul, 2019); in addition to one achromatic and two isoluminant color conditions, we also tested combinations of these. We found that the weakest sensations of luster were produced with pure chromatic stimuli. However, we found no obvious differences between the strength of perceived luster in pure achromatic stimuli and the luster perceived in stimuli with identical luminance differences that additionally comprised an interocular difference in chromaticity—which would be more indicative of a winner-take-all type of integration. In future experiments, we will test how interocular conflict signals from the different mechanisms will be combined by systematically varying the interocular differences across all dimensions in color space.

Conclusions

In this study, two psychophysical experiments were conducted to address the question of how interocular differences in chromatic contrast affect the strength of perceived luster in a series of isoluminant center-ring-surround stimuli. The strong similarities between the data trends of the present study and those of our previous study with achromatic stimuli (Wendt & Faul, 2022a) indicate that binocular luster is mediated by similar processes in both cases. Both cases are compatible with the idea that a low-level binocular conflict mechanism represents the neural basis for binocular luster, integrating the signals from monocular contrast detector cells at corresponding retinal locations. The data also suggest that the underlying mechanism is much more sensitive to monocular contrast signal combinations with opposite polarities than to interocular pairings with equal signs. This conclusion is supported by the results of a test of a modified version of our interocular conflict model that is based on the monocular signals from different types of color-responsive double-opponent cells. However, the spatial properties of the receptive fields of the monocular cells involved in the generation of the luster phenomenon remain to be clarified. Our empirical luster data could be predicted equally well with a chromatic model based on signals from cells with an antagonistic center-surround organization of their receptive fields (simulated with a Laplacian of Gaussian filter kernel) and on signals from orientation-selective cells with a side-by-side layout of the antagonistic areas of their receptive fields (simulated with a filter kernel based on the first derivative of a Gaussian).

Keywords: binocular luster, color vision, chromatic contrast, interocular conflict

Acknowledgments

The authors thank Alena Rech for her help in conducting the experiments and two anonymous reviewers for their helpful comments on an earlier draft of this paper.

Funded by the Deutsche Forschungsgemeinschaft (DFG, German Research Foundation) – 519638685.

Commercial relationships: none.
Corresponding author: Gunnar Wendt.
Email: gunwendt@psychologie.uni-kiel.de.
Address: Universität Kiel, Kiel, Germany.

References

Anstis, S. M. (2000). Monocular luster from flicker. *Vision Research, 40*(19), 2551–2556.

Brainard, D. H. (1989). Calibration of a computer controlled color monitor. *Color Research and Application, 14*, 23–34.

Brewster, D. (1861). On binocular luster. *Report of British Association, 2*, 29–31.

Conway, B. R. (2009). Color vision, cones, and color-coding in the cortex. *The Neuroscientist, 15*(3), 275–290.

Conway, B. R., & Livingstone, M. S. (2006). Spatial and temporal properties of cone signals in alert macaque primary visual cortex. *The Journal of Neuroscience, 26*(42), 10826–10846.

De, A., & Horwitz, G. D. (2021). Spatial receptive field structure of double-opponent cells in macaque V1. *Journal of Neurophysiology, 125*(3), 843–857.

de Weert, C. M. (1979). Colour contours and stereopsis. *Vision Research, 19*(5), 555–564.

Dove, H. W. (1851). Ueber die Ursachen des Glanzes und der Irradiation, abgeleitet aus chromatischen Versuchen mit dem Stereoskop. *Poggendorffs Annalen, 83*, 169–183.

Formankiewicz, M. A., & Mollon, J. D. (2009). The psychophysics of detecting binocular discrepancies of luminance. *Vision Research, 49*(15), 1929–1938.

Gegenfurtner, K. R. (2003). Cortical mechanisms of colour vision. *Nature Reviews Neuroscience, 4*(7), 563–572.

Georgeson, M. A., Wallis, S. A., Meese, T. S., & Baker, D. H. (2016). Contrast and luster: A model that accounts for eleven different forms of contrast discrimination in binocular vision. *Vision Research, 129*, 98–118.

Goncalves, N. R., & Welchman, A. E. (2017). "What not" detectors help the brain see in depth. *Current Biology, 27*(10), 1403–1412.

Henriksen, S., & Read, J. C. A. (2016). Visual perception: A novel differencing channel in binocular vision. *Current Biology, 26*(12), R500–R503.

Hetley, R. S., & Stine, W. W. (2019). At least two distinct mechanisms control binocular luster, rivalry, and perceived rotation with contrast and average luminance disparities. *PLoS One, 14*(5), 1–24.

Horwitz, G. D. (2020). Signals related to color in the early visual cortex. *Annual Review of Vision Science, 6*, 287–311.

Howard, I. P. (1995). Depth from binocular rivalry without spatial disparity. *Perception, 24*(1), 67–74.

Ishihara, S. (1967). *Tests for colour-blindness,* 24 plates edition. Tokyo: Kanehara Shuppan Co.

Jennings, B. J., & Kingdom, F. A. A. (2016). Detection of between-eye differences in color: Interactions with luminance. *Journal of Vision, 16*(3):23, 1–12, https://doi.org/10.1167/16.3.23.

Jimenéz, J. R., Rubino, M., Hita, E., & Jiménez Del Barco, L. (1997). Influence of the luminance and opponent chromatic channels on stereopsis with random-dot stereograms. *Vision Research, 37*(5), 591–596.

Johnson, E. N., Hawken, M. J., & Shapley, R. (2001). The spatial transformation of color in the primary visual cortex of the macaque monkey. *Nature Neuroscience, 4*(4), 409–416.

Johnson, E. N., Hawken, M. J., & Shapley, R. (2008). The orientation selectivity of color-responsive neurons in macaque V1. *Journal of Neuroscience, 28*(32), 8069–8106.

Jung, W. S., Moon, Y. G., Park, J. H., & Song, J. K. (2013). Glossiness representation using binocular color difference. *Optics Letters, 38*(14), 2584–2587.

Katyal, S., Engel, S. A., He, B., & He, S. (2016). Neurons that detect interocular conflict during binocular rivalry with EEG. *Journal of Vision, 16*(3):18, 1–12, https://doi.org/10.1167/16.3.18.

Katyal, S., Vergeer, M., He, S., He, B., & Engel, S. A. (2018). Conflict-sensitive neurons gate interocular suppression in human visual cortex. *Scientific Reports, 8*(1), 1239.

Kiesow, F. (1920). Osservazioni sopra il rapporto tra due oggetti visti separatamente coi due occhi. *Archivio italiano di psicologia generale e del lavoro, 1*, 3–38, 239–290.

Kingdom, F. A. A. (2012). Binocular vision: The eyes add and subtract. *Current Biology, 22*(1), R22–R24.

Kingdom, F. A. A., Jennings, B. J., & Georgeson, M. A. (2018). Adaptation to interocular difference. *Journal of Vision, 18*(5):9, 1–11, https://doi.org/10.1167/18.5.9.

Kingdom, F. A. A., Read, J. C. A., Hibbard, P. B., & May, K. A. (2022). Special issue: Coding strategies in binocular vision and stereopsis. *Vision Research, 193*, 107989.

Kingdom, F. A. A., Seulami, N. M., Jennings, B. J., & Georgeson, M. A. (2019). Interocular difference thresholds are mediated by binocular differencing, not summing channels. *Journal of Vision, 19*(14):18, 1–15, https://doi.org/10.1167/19.14.18.

Kingdom, F. A. A., & Simmons, D. R. (1996). Stereoacuity and colour contrast. *Vision Research, 36*(9), 1311–1319.

Lindeberg, T. (2013). A computational theory of visual receptive fields. *Biological Cybernetics, 107*(6), 589–635.

Lindeberg, T. (2021). Normative theory of visual receptive fields. *Heliyon, 7*(1), e05897.

Lu, C., & Fender, D. H. (1972). The interaction of color and luminance in stereoscopic vision. *Investigative Ophthalmology, 11*(6), 482–490.

MacLeod, D. I. A., & Boynton, R. M. (1979). Chromaticity diagram showing cone excitations by stimuli of equal luminance. *Journal of the Optical Society of America, 69*(8), 1183–1186.

Malkoc, G., & Kingdom, F. A. A. (2012). Dichoptic difference thresholds for chromatic stimuli. *Vision Research, 62*, 75–83.

Mausfeld, R., & Niederée, R. (1993). An inquiry into relational concepts of colour, based on incremental principles of colour coding for minimal relational stimuli. *Perception, 22*(4), 427–462.

Mausfeld, R., Wendt, G., & Golz, J. (2014). Lustrous material appearances: Internal and external

constraints on triggering conditions for binocular luster. *I-Perception, 5*(1), 1–19.

Niederée, R. (2010). More than three dimensions: What continuity considerations can tell us about perceived color. In J. Cohen & M. Matthen (Eds.), *Color ontology and color science*. Cambridge, MA: MIT Press; 115–138.

Pieper, W., & Ludwig, I. (2001). Binocular vision: Rivalry, stereoscopic luster, and sieve effect. *Perception, 30*(1), 75.

Prince, S. J. D., Cumming, B. G., & Parker, A. J. (2002). Range and mechanism of encoding of horizontal disparity in macaque V1. *Journal of Neurophysiology, 87*(1), 209–221.

Qiu, S. X., Caldwell, C. L., You, J. Y., & Mendola, J. D. (2020). Binocular rivalry from luminance and contrast. *Vision Research, 175*, 41–50.

Read, J. C. A., & Cumming, B. G. (2003). Testing quantitative models of binocular disparity selectivity in primary visual cortex. *Journal of Neurophysiology, 90*(5), 2795–2817.

Read, J. C. A., & Cumming, B. G. (2004). Ocular dominance predicts neither strength nor class of disparity selectivity with random-dot stimuli in primate V1. *Journal of Neurophysiology, 91*(3), 1271–1281.

Read, J. C. A., & Cumming, B. G. (2007). Sensors for impossible stimuli may solve the stereo correspondence problem. *Nature Neuroscience, 10*(10), 1322–1328.

Ruete, C. G. T. (1860). *Das Stereoscop*. Leipzig: Teubner.

Sachsenweger, R. (1960). Studien über den stereoskopischen Glanz. *Albert von Graefes Archiv für Ophthalmologie, 162*, 518–526.

Said, C. P., & Heeger, D. J. (2013). A model of binocular rivalry and cross-orientation suppression. *PLoS Computational Biology, 9*(3), e1002991.

Schiller, P. H. (1992). The ON and OFF channels of the visual system. *Trends in Neurosciences, 15*(3), 86–92.

Schluppeck, D., & Engel, S. A. (2002). Color opponent neurons in V1: A review and model reconciling results from imaging and single-unit recording. *Journal of Vision, 2*(6), 480–492, https://doi.org/10.1167/2.6.5.

Shapley, R., & Hawken, M. (2002). Neural mechanisms for color perception in the primary visual cortex. *Current Opinion in Neurobiology, 12*(4), 426–432.

Shapley, R., & Hawken, M. (2011). Color in the cortex: Single- and double-opponent cells. *Vision Research, 51*(7), 701–717.

Sheedy, J. E., & Stocker, E. G. (1984). Surrogate color vision by luster discrimination. *American Journal of Optometry and Physiological Optics, 61*(8), 499–505.

Simmons, D. R., & Kingdom, F. A. A. (1994). Contrast thresholds for stereoscopic depth identification with isoluminant and isochromatic stimuli. *Vision Research, 34*(22), 2971–2982.

Solomon, S. G., & Lennie, P. (2007). The machinery of colour vision. *Nature Reviews, 8*(4), 275–286.

Stockman, A., & Sharpe, L. T. (2000). The spectral sensitivities of the middle- and long-wavelength-sensitive cones derived from measurements in observers of known genotype. *Vision Research, 40*(13), 1711–1737.

Thorell, L. G., De Valois, R. L., & Albrecht, D. G. (1984). Spatial mapping of monkey V1 cells with pure color and luminance stimuli. *Vision Research, 24*(7), 751–769.

Venkataramanan, K., Gawde, S., Hathibelagal, A. R., & Bharadwaj, S. R. (2021). Binocular fusion enhances the efficiency of spot-the-difference gameplay. *PLoS One, 16*(7), e0254715.

Vladusich, T., Lucassen, M. P., & Cornelissen, F. W. (2007). Brightness and darkness as perceptual dimensions. *PLoS Computational Biology, 3*(10), 1849–1858.

von Helmholtz, H. (1867). *Handbuch der physiologischen Optik*. Hamburg: Voss.

Wang, Q., & Spratling, M. W. (2016). Contour detection in colour images using a neurophysiologically inspired model. *Cognitive Computation, 8*, 1027–1035.

Wendt, G., & Faul, F. (2019). Differences in stereoscopic luster evoked by static and dynamic stimuli. *i-Perception, 10*(3), 1–26.

Wendt, G., & Faul, F. (2020). The role of contrast polarities in binocular luster: Low-level and high-level processes. *Vision Research, 176*, 141–155.

Wendt, G., & Faul, F. (2022a). A simple model of binocular luster. *Journal of Vision, 22*(10):, 1–26, https://doi.org/10.1167/jov.22.10.6.

Wendt, G., & Faul, F. (2022b). Binocular luster – A review. *Vision Research, 194*, 108008.

Wienbar, S., & Schwarz, G. (2018). The dynamic receptive fields of retinal ganglion cells. *Progress in Retinal and Eye Research, 67*, 102–117.

Wolfe, J. M., & Franzel, S. L. (1988). Binocularity and visual search. *Perception & Psychophysics, 44*(1), 81–93.

Wundt, W. (1862). Ueber die Entstehung des Glanzes. *Poggendorffs Annalen, 116*, 627–631 .

Yoonessi, A., & Kingdom, F. A. A. (2009). Dichoptic difference thresholds for uniform color changes applied to natural scenes. *Journal of Vision, 9*(2):3, 1–12, https://doi.org/10.1167/9.2.3.

Zhang, H. (2015). *Spectacularly binocular: Exploiting binocular luster effects for HCI applications* (unpublished doctoral dissertation). Singapore: National University of Singapore.

Appendix A

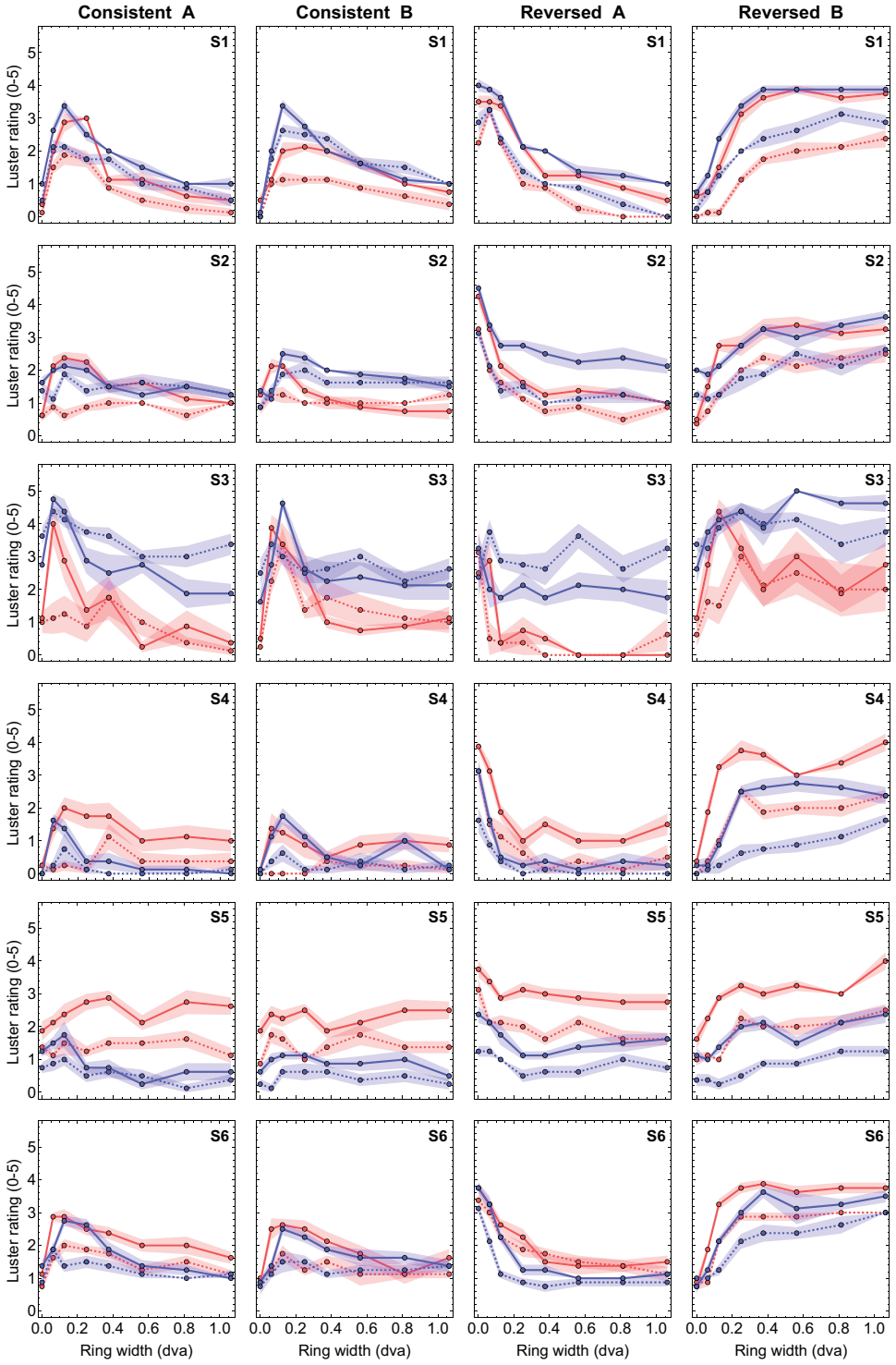

Figure A1. Results of the rating task of Experiment 1. For each contrast condition (columns) and each subject (rows) the mean rating values are plotted as a function of ring width. Red curves show the results for the RG color condition, blue curves those for the BY color condition. Solid lines refer to the high DCD condition, dashed lines to the low DCD condition. Transparent areas represent 1 *SEM* in both directions.

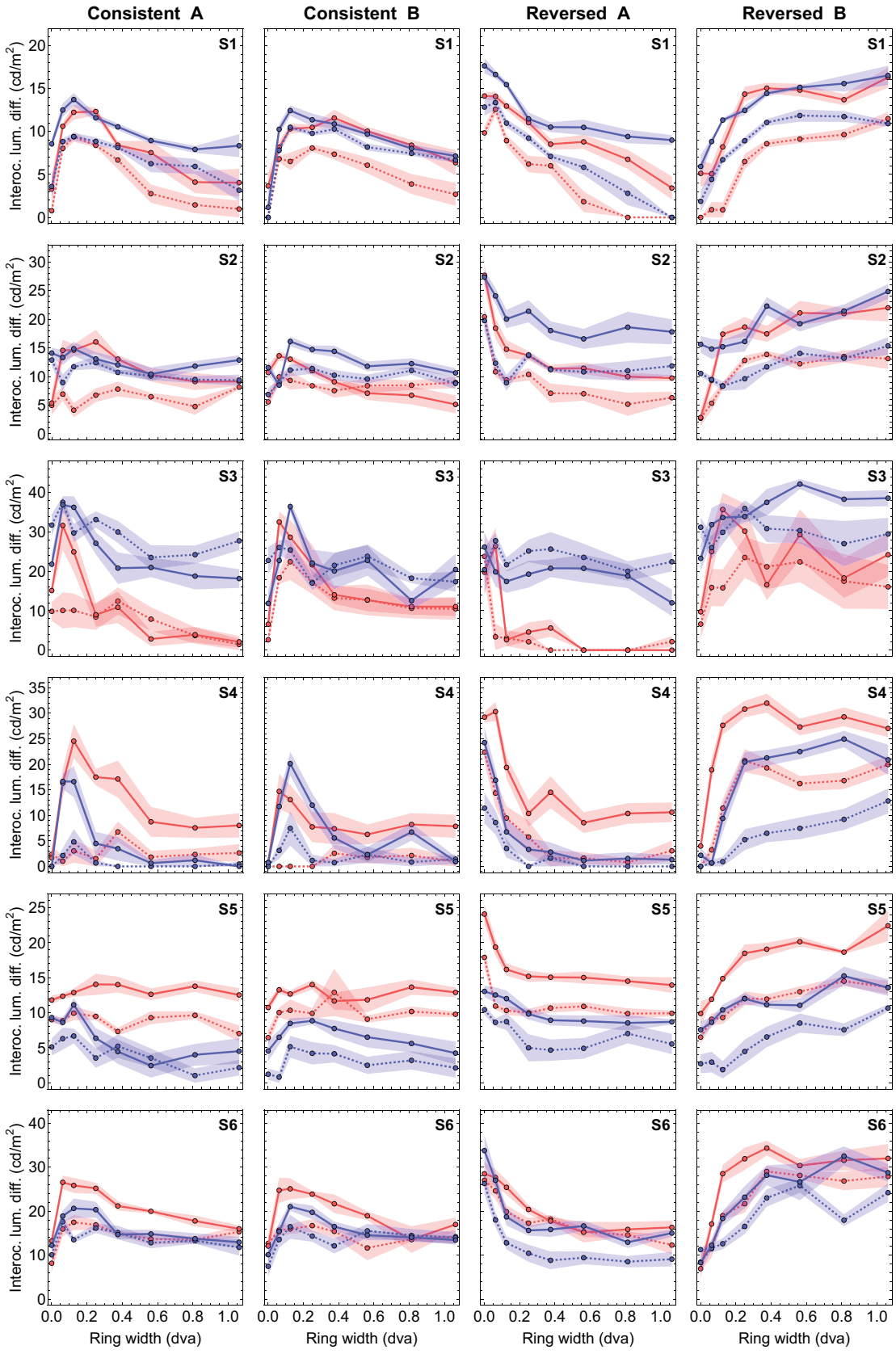

Figure A2. Results of the matching task of Experiment 1. For each contrast condition (columns) and each subject (rows) the mean settings of the matching stimulus are plotted as a function of ring width. Red curves show the results for the RG color condition, blue curves those for the BY color condition. Solid lines refer to the high DCD condition, dashed lines to the low DCD condition. Transparent areas represent 1 *SEM* in both directions.

Appendix B

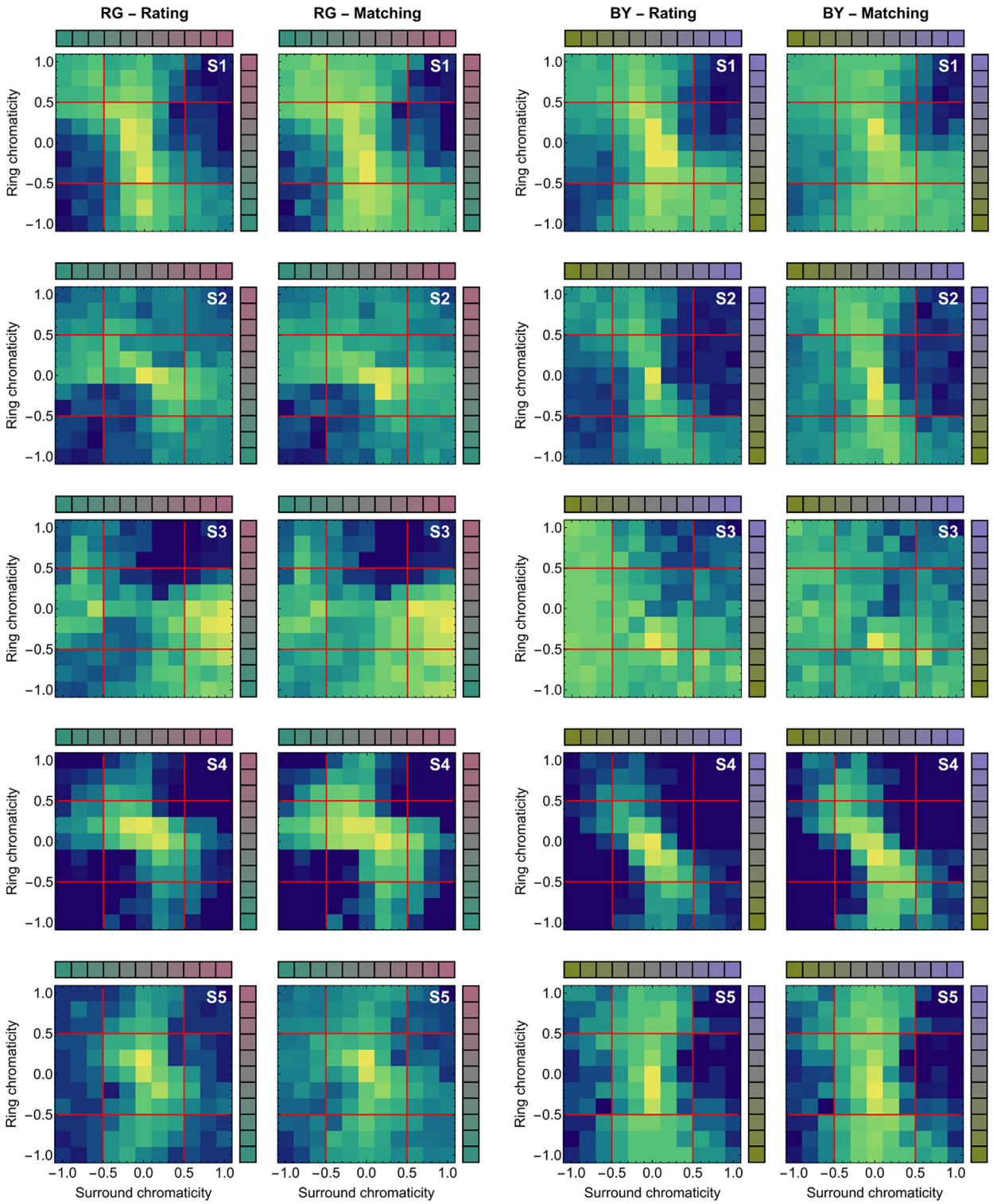

Figure B1. Results of Experiment 2 for the five subjects S1 to S5 (rows). The results for the RG color conditions are shown in the left pair, the results for the BY color conditions in the right pair of diagrams. See Figure 7 and the main text for further details.